Published in final edited form as:

Mol Cell Neurosci. 2022 July ; 121: 103756. doi:10.1016/j.mcn.2022.103756.

Hyperactivity of Purkinje cell and motor deficits in *C9orf72* knockout mice

Yuning Liu[1,2], **Hong Xing**[1], **Alexis F Ernst**[1], **Canna Liu**[1], **Christian Maugee**[1,2], **Fumiaki Yokoi**[1], **Madepalli Lakshmana**[3], **Yuqing Li**[1,*]

[1]Norman Fixel Institute for Neurological Diseases, Department of Neurology, College of Medicine, University of Florida, Gainesville, FL, United States.

[2]Genetics Institute, University of Florida, Gainesville, FL, United States.

[3]Department of Immunology and Nano-Medicine, The Herbert Wertheim College of Medicine, Florida International University, Miami, FL, United States.

Abstract

A hexanucleotide (GGGGCC) repeat expansion in the first intron of the *C9ORF72* gene is the most frequently reported genetic cause of amyotrophic lateral sclerosis (ALS) and frontotemporal dementia (FTD). The cerebellum has not traditionally been thought to be involved in the pathogenesis of *C9ORF72*-associated ALS/FTD, but recent evidence suggested a potential role. *C9ORF72* is highly expressed in the cerebellum. Decreased *C9ORF72* transcript and protein levels were detected in the postmortem cerebellum, suggesting a loss-of-function effect of *C9ORF72* mutation. This study investigated the role of loss of *C9ORF72* function using a *C9orf72* knockout mouse line. *C9orf72* deficiency led to motor impairment in rotarod, beam-walking, paw-print, open-field, and grip-strength tests. Purkinje cells are the sole output neurons in the cerebellum, and we next determined their involvement in the motor phenotypes. We found hyperactivity of Purkinje cells in the *C9orf72* knockout mouse accompanied by a significant increase of the large-conductance calcium-activated potassium channel (BK) protein in the cerebellum. The link between BK and Purkinje cell firing was demonstrated by the acute application of the BK activator that increased the firing frequency of the Purkinje cells *ex vivo*. *In vivo* chemogenetic activation of Purkinje cells in wild-type mice led to similar motor deficits in rotarod and beam-walking tests. Our results highlight that C9ORF72 loss alters the activity of the Purkinje cell and potentially the pathogenesis of the disease. Manipulating the Purkinje cell firing or cerebellar output may contribute to C9ORF72-associated ALS/FTD treatment.

Keywords

C9orf72; Purkinje cell; BK channel; Hyperactivity; Motor behavior

[*]**Correspondence to** Dr. Yuqing Li, Department of Neurology, College of Medicine, University of Florida, PO Box 100236, Gainesville, FL 32610-0236, USA. yuqingli@ufl.edu; Phone 1-352-273-6546; Fax: 352-273-5989.

Declarations of interest: None

1. Introduction

Amyotrophic lateral sclerosis (ALS) is a heterogeneous lethal neurodegenerative disease characterized by the degeneration of both upper and lower motor neurons (Hardiman et al., 2017). Frontotemporal dementia (FTD) is a spectrum of early-onset, non-Alzheimer's dementia characterized by degeneration of the frontal and anterior temporal cortex (Olney et al., 2017). In the last decade, significant findings support the shared clinicopathology between ALS and FTD, such as cognitive and behavioral impairments and TAR DNA-binding protein 43 (TDP-43) inclusions (Arai et al., 2006; Neumann et al., 2006). The later discovery of a hexanucleotide (GGGGCC, G4C2) repeats expansion in a non-coding region of the *C9ORF72* gene was identified as the most common genetic cause of ALS/FTD (DeJesus-Hernandez et al., 2011; Renton et al., 2011). This pathogenic expansion accounts for approximately 5-10% of sporadic ALS, 40% of familial ALS, and 25% of FTD (Majounie et al., 2012). The GGGGCC repeats are located in the first intron of the *C9ORF72* gene. The repeat length is typically no more than 23 in healthy individuals (DeJesus-Hernandez et al., 2011). However, in C9ORF72 ALS/FTD patients, the hexanucleotide repeats can expand to hundreds or even thousand (DeJesus-Hernandez et al., 2011; Renton et al., 2011).

How the pathogenic hexanucleotide repeats lead to ALS/FTD is being heavily debated. There have been three major, but non-exclusive mechanisms proposed: loss of function of the C9ORF72 protein caused by haploinsufficiency of *C9ORF72* mRNA (DeJesus-Hernandez et al., 2011; Gijselinck et al., 2012; Renton et al., 2011; Waite et al., 2014; Xiao et al., 2015), a toxic gain of function from bidirectionally transcribed sense (GGGGCC) and antisense (GGCCCC) transcripts that form RNA foci (DeJesus-Hernandez et al., 2011; Swinnen et al., 2020; Zu et al., 2013), and toxic gain of function from dipeptide repeat proteins (DPRs) produced by repeat-associated non-ATG (RAN) translation (Freibaum & Taylor, 2017; Mori et al., 2013; Zu et al., 2013). These mechanisms are all likely to contribute to disease pathogenesis; therefore, it is crucial to determine their specific roles in the C9ORF72-associated ALS/FTD pathophysiology.

The function of the C9ORF72 protein is not known. C9orf72 knockout and knockdown rodent models have been developed to determine its function and evaluate the role of loss of function in the pathogenesis of the disease. Surprisingly, most knockout models report immune dysfunctions and lysosomal and autophagy-related alterations but lack motor phenotypes (Braems et al., 2020; Pang & Hu, 2021). On the other hand, two independent GGGGCC repeat expansion transgenic mouse model studies revealed that loss of function of C9orf72 in mice exacerbates motor deficits, highlighting the importance of the C9orf72 haploinsufficiency in pathogenesis (Shao et al., 2019; Zhu et al., 2020).

The cerebellum is critically important in motor learning and posture control by providing feedback and fine-tuning for motor output (Ito, 2008). The cerebellum could play an essential role in *C9ORF72*-associated ALS/FTD (Prell & Grosskreutz, 2013). The level of C9ORF72 protein in the cerebellum is the highest among brain regions, indicating C9ORF72 in the cerebellum is essential for normal physiological function (Renton et al., 2011; Waite et al., 2014). In presymptomatic *C9ORF72* mutation carriers, several

neuroimaging studies show significant grey matter atrophy in the cerebellum (Bocchetta et al., 2016; Cash et al., 2018; Irwin et al., 2013; Mahoney et al., 2012; Panman et al., 2019; Papma et al., 2017; Tan et al., 2014). Besides, cerebellar hypermetabolism is detected in *C9ORF72* patients (Castelnovo et al., 2019; Cistaro et al., 2014). In addition to neuroimaging studies, an impairment of cerebellar-specific tasks in *C9ORF72* mutation carriers has been reported (Hornberger, 2012). Furthermore, patients with *C9ORF72* mutation develop classic cerebellar symptoms, such as ataxia, indicating that the toxic *C9ORF72* repeats expansion may affect cerebellar function (Corcia et al., 2016; Meloni et al., 2017).

Pathological studies further suggest the involvement of the cerebellum in C9ORF72-associated ALS/FTD through toxic gain of function and loss of function mechanisms. First, sense and antisense RNA foci comprising *C9ORF72* repeat RNA are found predominantly within neuronal nuclei in the cerebellum of *C9ORF72* patients (Cooper-Knock et al., 2015; DeJesus-Hernandez et al., 2017; Gendron et al., 2013; Lagier-Tourenne et al., 2013; Mizielinska et al., 2013). Second, protein assays using the postmortem cerebellum of healthy controls and *C9ORF72* cases uncovered DPR protein pathology (Ash et al., 2013; Baborie et al., 2015; Gendron et al., 2015; Mackenzie et al., 2015; Mann et al., 2013; Mori et al., 2013; Ramos-Campoy et al., 2018). Finally, the cerebellum is also associated with the haploinsufficiency of C9ORF72 in the *C9ORF72*-associated ALS/FTD. Transcriptional studies showed reduced levels of the *C9ORF72* transcript variants in the cerebellum of *C9ORF72* expansion carriers compared with controls (Belzil et al., 2013; Donnelly et al., 2013; Fomin et al., 2018; Mori et al., 2013; van Blitterswijk et al., 2015; Waite et al., 2014). There is a significant association between survival and expression level of the *C9ORF72* transcript in the cerebellum, such that expression levels greater than the 25^{th} percentile of the patients conferred a survival advantage (van Blitterswijk et al., 2015). Furthermore, reduced C9ORF72 protein levels in the cerebellum were detected by two studies when comparing *C9ORF72* mutation carriers to controls (Frick et al., 2018; Sivadasan et al., 2016). These results highlight the critical role of the cerebellum in the *C9ORF72*-mediated disease. However, how the C9ORF72 protein is related to the function of the cerebellum, especially Purkinje cells, the sole projection neurons from the cerebellar cortex, and its involvement in disease pathogenesis are still unknown. In this study, we used an existing C9orf72 knockout mouse model to determine the functional changes of cerebellar Purkinje cells and the associated motor behaviors.

2. Materials and methods

2.1. Animals

All experiments were carried out by investigators blind to the genotypes and in compliance with the the ARRIVE guidelines, and be carried out in accordance with the USPHS Guide for Care and Use of Laboratory Animals and approved by the IACUC at the University of Florida. The mice were housed with *ad libitum* access to food and water under 12 hours-light and 12 hours-dark.

C9orf72 null mice (*C9orf72* KO mice) were from Jackson Lab (Stock No. 027068: C57BL/6J-*C9orf72*^{em5Lutzy}/J) (O'Rourke et al., 2016). Heterozygous knockout (KO) mice were

interbred to produce experimental homozygous KO mice and the wild-type littermate (WT) controls. Genotyping for *C9orf72* KO mice was performed by PCR using tail DNA and a set of 26371 (5′- AAT GGC TGA ACC TGA TCA CTG -3′) and 26372 (5′- AAA GGT AGC CGC CAA CAA G -3′) primers.

To selectively activate Purkinje cell firing, we used a DREADD mouse line conditionally expressing a hM3Dq receptor (CAG-LSL-HA-hM3Dq-pta-mCitrine; Jackson Lab. stock no. 026220). We crossed this line with the *Pcp2-cre* mouse line (BAC-Pcp2-IRES-Cre; Jackson laboratory stock no. 010536) that expresses Cre recombinase specifically in cerebellar Purkinje cells (Zhang et al., 2004) to generate *Pcp2-cre*/hM3Dq double mutant mice. Upon removal of floxed stop cassette by Cre-mediated recombination, the Gq-coupled hM3Dq was expressed, and the administration of CNO activated the Purkinje cell firing. There is no endogenous receptor of CNO in mice, and injection of CNO will cause little adverse effect at low concentrations (MacLaren et al., 2016). Genotyping for *Pcp2-cre*/hM3Dq mice was performed by multiplex PCR using tail DNA and a set of primers (22888: GTGGTACCGTCTGGAGAGGA; 22887: CGCCACCATGTACCCATAC) for hM3Dq and a set of creA and cre6 primers for *cre* (Yokoi et al., 2011).

This study followed the recommended heterogenization of study samples with various conditions (Voelkl et al., 2020). Adult mice of different ages were used for all behavioral tests. The data were analyzed with age as a covariate.

2.2. Electrophysiological recording

2.2.1. Brain slice preparation—Cell-attached slice recordings of Purkinje cells were obtained from 3 adult male *C9orf72* KO mice and 4 male WT littermates. The slice preparation was described previously (Liu et al., 2020; Lyu et al., 2019). Briefly, the brains were rapidly removed and chilled in the ice-cold cutting solution containing (in mM) 180 sucrose, 2.5 KCl, 1.25 NaH_2PO_4, 25 $NaHCO_3$, 1 $CaCl_2$, 10 $MgCl_2$, and 10 D-glucose and were oxygenated with 95% O_2-5% CO_2 (pH 7.35~7.45). Parasagittal 300 μm-thick cerebellar brain slices were obtained with a Vibratome (LEICA VT 1000S, Leica Microsystems) in the same ice-cold cutting solution. Slices were first incubated on a brain slice keeper (AutoMate Scientific, Inc.) and covered by a thin layer of artificial cerebrospinal fluid (ACSF) containing (in mM) 126 NaCl, 2.5 KCl, 1.25 NaH_2PO_4, 25 $NaHCO_3$, 2 $CaCl_2$, 5 $MgCl_2$, and 10 D-glucose and were constantly oxygenated at 35°C for 60 minutes. After a minimum of 60 minutes of incubation, a slice was transferred to a submerged recording chamber with the continuous flow (1.5 ml/min) of oxygenated ACSF at room temperature until electrophysiological recording.

2.2.2. Cell-attached recordings—The Purkinje cell recorded was located in the apex and the bank of the cerebellar vermis lobules 4 to 6, and it was identified by infrared visualization in parasagittal cerebellar slices. Lobules 4 to 6 were selected because they receive inputs from hind limbs. The cell-attached recordings were performed as previously described (Lyu et al., 2019). Briefly, the spontaneous action potentials were recorded by the voltage clamp at cell-attached mode with infrared-differential interference contrast microscopy (IR-DIC) and video microscopy (Axioskop-FS; Carl Zeiss, Jena, Germany) with

a 40× water-immersion lens and an Axopatch 1D amplifier (Axon Instruments, Foster City, CA). The patch electrodes had a resistance of 5–10 MΩ when filled with a K-gluconate-based intracellular solution containing (in mM): 112.5 K-gluconate, 4 NaCl, 17.5 KCl, 0.5 $CaCl_2$, 5 MgATP, 1 NaGTP, 5 EGTA, 10 HEPES, and pH 7.2 (osmolality 270–280 mOsm/l). Positive pressure was applied to the patch electrode as it approached the Purkinje cell. Suction was applied to the electrode to create a seal (> 5 GΩ) between the recording pipette and the cell membrane. Action potential current was recorded in the voltage-clamp mode that maintained an average of 0 pA holding current. Picrotoxin (10 μM), CGP55845 (1 μM), and kynurenic acid (5mM) were added to the ACSF to block synaptic transmission (Fremont et al., 2017).

NS11021 (1 μM, Tocris Bioscience) was added to the recording chamber for 2 minutes after the cell was recorded for 5 minutes. An additional 2 minutes was recorded to determine the washout. The firing pattern before drug treatment was quantified after the first minute of recording until the drug entered the recording chamber. The treatment effect was measured from 30 seconds until 2 minutes after the drug entered the recording chamber.

All experiments were conducted at 35°C ± 0.5°C by a dual automatic temperature controller (TC-344B, Harvard Apparatus). The recording data were acquired using pClamp 10 software (Molecular Devices), and signals were filtered at 5 kHz and digitized at 10 kHz with a DigiData 1440 (Molecular Devices). The data were further analyzed by the Mini Analysis Program (Synaptosoft).

2.2.3. Whole-cell recordings—After recording the action potentials, the attached membrane was broken through by suction from the microelectrode, and electrode access resistance was maintained throughout at <30 MΩ. Action potential for current step recording was triggered using depolarizing currents steps of 300 ms. Furthermore, whole-cell recordings were made from Purkinje cells in current-clamp mode to validate the chemogenetic activation of Purkinje cell activity by clozapine-N-oxide (CNO) bath application to the brain slices derived from the *Pcp2-cre*/hM3Dq mice. Patch electrodes had a resistance of 5–10 MΩ when filled with intracellular solution containing (in mM): 112.5 K-gluconate, 4 NaCl, 17.5 KCl, 0.5 CaCl2, 5 MgATP, 1 NaGTP, 5 EGTA, 10 HEPES, and pH 7.2 (osmolality 270–280 mOsm/l). Series resistance was 9–15 MΩ, and cells were rejected if they changed >10% throughout the recording session. After recording the baseline, CNO was applied to bath (1 μM, 1 min) followed by ACSF washed out to test the effect of CNO on Purkinje cell firing.

2.3. Brain histology

Adult *Pcp2-cre*/hM3Dq mice were anesthetized and perfused with PBS followed by 4% paraformaldehyde. The brains were dissected and soaked in 4% paraformaldehyde overnight and then in 30% sucrose in PBS. Coronal sections (35 μm thickness) were obtained using a freezing sliding microtome. The slices were mounted and covered with the Vectashield mounting medium and stored at 4°C overnight. The positive cells were identified using the FITC filter for mCitrine and the MBF Bioscience Neurolucida 7 software (MicroBrightFields Bioscience).

2.4. Behavioral analysis

A group of 21 adult *C9orf72* KO mice and 19 WT littermates of either sex were assessed by a behavioral test battery for motor performance consisting of a body form assessment, accelerated rotarod, beam-walking, open-field, paw-print gait analysis, and grip-strength tests. Tests were performed in the above order, with mice resting for up to two weeks in between the tests.

Another group of 14 adult *Pcp2-cre*/hM3Dq mice was randomly assigned to age-matched groups consisting of 8 mice in the CNO group (0.2 mg/kg) and 6 mice in the saline group. The CNO solution in saline or saline (0.9% NaCl) was injected intraperitoneally once on each test day about 1 hour before the beginning of the test. Motor behaviors were assessed by semi-quantitative assessments, accelerated rotarod, and beam-walking tests.

2.4.1. Body form assessment—Body form assessment of movement disorders was performed as described earlier (Dang et al., 2005; Fernagut et al., 2002). Mice were placed individually on the table. Truncal dystonia and balance adjustments to a postural challenge were examined. Truncal dystonia was assessed as the flexed posture. The postural challenge was observed by flipping the mouse onto its back, and its capability of righting was noted.

2.4.2. Accelerated rotarod test—The accelerated rotarod test assesses the ability of mice to maintain balance and coordination on an accelerating rotating rod. The mice were examined with an accelerating rotarod (Ugo Basile) as previously described (Liu et al., 2021). The apparatus started at an initial speed of 4 rpm, and then each mouse was put on the same slot one by one to minimize the variations. The rod speed was gradually accelerated at a rate of 0.2 rpm/s. The latency to fall was measured with a cutoff time of 3 min at a final rate of 40 rpm. Mice were tested for three trials each day for two days. The trials within the same day were performed at about 1-hour intervals.

2.4.3. Beam-walking test—The beam-walking test was performed within the last 8 hours of the light period after acclimation to a sound-attenuated testing room for 1 hour as described earlier (Dang et al., 2005). The mice were trained to traverse a medium square beam (14 mm wide) in three consecutive trials each day for two days, and they were tested twice each on the medium square beam and a medium round beam (17 mm diameter) on the third day. The mice were then tested twice each on a small round beam (10 mm diameter) and a small square beam (7 mm wide) on the fourth day. The number of hind paw slips on each side was counted by investigators blind to the genotypes. All four beams were 100 cm long, and the slips traversing the middle 80 cm were counted.

2.4.4. Open-field test—The open-field test was performed during the light period, as previously described (Liu et al., 2021). Each mouse in the same group was placed in the center of a VersaMax Legacy open field apparatus connected to a computerized Digiscan System (Accuscan Instruments, Inc. OH) and continuously monitored for 30 minutes at 1 min intervals. A bright illumination (approximately 1k lux at the center by a 60W white bulb) was focused on the center of each field.

2.4.5. Paw-print gait analysis—The paw-print test is an analysis of the animal's gait. A runway with a dark goal box at the end was lined with a sheet of white paper (Carter et al., 2001). The fore and hind paws of the mice were painted with water-soluble, non-toxic paint of different colors. Mice walked across the runway and into the goal box. One set of prints was collected for each animal after it walked continuously across the runway. The four center pairs of hind and forepaw prints of each set were analyzed for stride length, forelimb and hind limb base lengths, and distance of overlap of the paws.

2.4.6. Grip strength test—To assess forelimb and hind limb strength, we used a grip strength meter (BIO-GS3, BIOSEB). The meter records the force of a metal grate being pulled in grams. To measure forelimb strength, we held the mice by their tail at an angle that prevented the hind limbs from grasping the metal grate and were quickly pulled back. To measure four-limb grip strength, we placed mice on the metal grid until they gripped it, and then they were gently pulled by the tail until they could no longer hold the grid. Each measurement was conducted three times, and the maximum force of the three trials was used for statistical analysis.

2.5. Western blot analysis

To quantify C9orf72 protein levels in the brain, WT and C9orf72 KO mice were euthanized with carbon dioxide, decapitated immediately. Their brains were rapidly dissected and separated on ice and placed into cold lysis buffer containing 1% Nonidet P-40, 50mM Tris-HCl, pH 8.0, 150 mM NaCl and 0.02% sodium azide with complete protease inhibitor mix for use in mammalian cells (cat # P8340, Sigma Aldrich) supplemented with 400 nM microcystin-LR and 0.5mM sodium vanadate. Samples were homogenized using Power Gen 125 homogenizer, ultracentrifuged at 120,000 rpm at 4°C for 20 minutes, denatured at 95°C for 10 minutes and the lysate samples were loaded into each well and subjected to SDS-PAGE electrophoresis. The proteins were then transferred onto PVDF membranes, blocked with 5% non-fat dry milk in TBS-T buffer, and incubated overnight with C9orf72 primary antibody (cat # GTX632041, GeneTex). Mouse monoclonal antibody against beta-actin (cat # A00702, GenScript USA) was used to detect actin as a loading control, followed by 1- to 2-hour incubation with HRP-conjugated mouse secondary antibody (cat # 115-035-146, Jackson ImmunoResearch Laboratories). The protein signals were detected using super signal west pico chemiluminescent substrate (cat # 34580, Thermo Fisher, USA). These methods are described in publications (Lakshmana et al., 2010; Wang et al., 2015).

To quantify Calcium-dependent potassium channel protein levels in the brain, we dissected and homogenized the cerebellum in 200 μl of ice-cold lysis buffer. The proteins were extracted in 1% Triton X-100-containing buffer and quantified as previously described (Yokoi et al., 2010). Protein samples from 7 adult KO and 6 WT littermates were separated on 10% sodium dodecyl sulfate-polyacrylamide gel electrophoresis (SDS-PAGE) and transferred to Millipore Immobilon–FL transfer PVDF membranes. The PVDF membranes were blocked with LI-COR Odyssey blocking buffer and incubated at 4°C overnight with mouse anti-Slo1/BKAlpha potassium channel antibody (UC Davis/NIH NeuroMab clone L6/60; 1:4,000 dilution), rabbit anti-KCNN2 (Kca2.2, SK2) antibody (Alomone lab, APC-028; 1:4,000 dilution), rabbit anti-$Na_V1.6$ (SCN8A) antibody (Alomone lab, ASC-009;

1:1,000 dilution), rabbit anti-K_V4.3 antibody (Alomone lab, APC-017; 1:500 dilution), or rabbit anti-glyceraldehyde-3-phosphate dehydrogenase (GAPDH) antibody (Santa Cruz, sc-25778; 1:1,000 dilution). LI-COR IRDye 800CW donkey anti-mouse IgG (H+L) or LI-COR IRDye 680RD donkey anti-rabbit IgG (H+L) were used when appropriate at the dilution of 1:15,556. The infrared emission signals were detected and recorded as digital data by an LI-COR Odyssey imaging system. The density of the corresponding protein band was normalized to those of GAPDH. Western blot analysis was performed in duplicate.

2.6. Statistical analysis

Data were analyzed by SAS/STAT mixed model for normally distributed data or GENMOD procedure (SAS) with log link for gamma distribution when they were not normally distributed (Yokoi et al., 2020). The SAS PROC GENMOD was selected due to its ability to handle nested data or repeated measurements and allow missing values and non-symmetrical research design. It can also deal with the data that are not normally distributed. Bodyweight and spleen weight were normally distributed and were analyzed by SAS/STAT mixed model with age as a continuous variable. Latency to fall in the accelerated rotarod test was not normally distributed and was analyzed using the GENMOD procedure (SAS). Slip numbers in the beam-walking test were analyzed using the GENMOD procedure with a negative binomial distribution (Dang et al., 2005). Paw-print data were tested for normality using the SAS statistical package. Stride and base were normally distributed and were analyzed by SAS/STAT mixed model, while overlap data was not normally distributed and was analyzed by the GENMOD procedure. Open-field and grip-strength data were normally distributed and analyzed by the SAS/STAT mixed model. Sex, age, and body weight were used as covariates in all behavioral analyses. Two-way interactions between genotype and other covariates were analyzed first. Electrophysiological recording data were tested for normality using the SAS statistical package. Cell-attached slice-recording data were processed using the Mini Analysis Program (Synaptosoft). The recorded neurons were nested within each animal (Lyu et al., 2019). Age was used as a continuous variable in all electrophysiological analyses. The Western blot signals were analyzed using the Student's t-test and the GENMOD procedure. Significance was assigned at $p \leq 0.05$.

3. Results

3.1. Motor deficits in *C9orf72* KO mice

C9orf72 KO mice were generated by interbreeding heterozygous KO mice (O'Rourke et al., 2016). Complete loss of C9orf72 protein was confirmed by western blot (Suppl. Fig. 1A). *C9orf72* KO mice were obtained with Mendelian distribution ($p = 0.99$, Fisher's exact test), suggesting that *C9orf72* KO mice are neither embryonic nor neonatal lethal. KO mice grew up to adulthood without noticeable developmental delay. Significantly enlarged spleens were found in KO mice (Suppl. Fig. 1B, $p < 0.001$, Mixed model) as reported previously (O'Rourke et al., 2016). However, we detected slightly decreased bodyweight of the *C9orf72* KO mice compared with WT littermates (Suppl. Fig. 1C, $p < 0.001$, GENMOD with a gamma distribution). Furthermore, we found that the KO mice did not gain their body weight with increased age (Suppl. Fig. 1D, slopes equal: $p = 0.006$, Linear regression).

Prior studies found mild motor phenotypes in *C9orf72* KO mouse models (Atanasio et al., 2016; Jiang et al., 2016). To assess an overall motor performance profile of *C9orf72* KO mice, we used a behavioral test battery consisting of a body form assessment, accelerated rotarod, beam-walking test, open-field, paw-print gait analysis, and grip-strength test. KO mice showed no deficits in the semi-quantitative assessments. All mice exhibited strong righting reflexes when tipped on their side.

The rotarod is a standard test that assesses motor coordination (Caston et al., 1995; Lalonde et al., 1995). There was a significantly decreased latency to fall in KO mice compared with WT mice (Fig. 1A, Mean ± SEM: WT: 153.98 ± 4.56, n = 19; KO: 141.28 ± 3.96, n = 21, $p = 0.032$, GENMOD with a gamma distribution). Sex differences have been found in the cerebellum (Nguon et al., 2005). The latency to fall data were further analyzed separately by sex. The male KO mice showed a significantly shorter latency to fall than male WT mice (Mean ± SEM: WT: 151.46 ± 7.64, n = 9; KO: 125.13 ± 7.13, n = 11, $p = 0.022$, GENMOD with a gamma distribution), suggesting motor deficits in male KO mice. On the other hand, there was no significant difference in the latency to fall between female WT and KO mice (Mean ± SEM: WT: 159.89 ± 4.69, n = 10; KO: 157.22 ± 3.95, n = 10, $p = 0.659$, GENMOD with a gamma distribution).

Motor coordination and balance were further analyzed by the beam-walking test (Carter et al., 1999). *C9orf72* KO mice showed a significant increase of slips (Fig. 1B, Mean ± SEM: WT: 0.22 ± 0.085, n = 19; KO: 0.59 ± 0.13, n = 21, $p = 0.019$, GENMOD with a negative binomial distribution), suggesting motor deficits in KO mice. The slip numbers were analyzed further in each sex. Male KO mice showed a significant increase in slip numbers in the beam-walking test (Mean ± SEM: WT: 0.23 ± 0.12, n = 9; KO: 0.89 ± 0.28, n = 11, $p = 0.025$). On the other hand, there was no significant difference in slip numbers between female WT and KO mice (Mean ± SEM: WT: 0.20 ± 0.10, n = 10; KO: 0.37 ± 0.11, n = 10, $p = 0.594$). We further analyzed the motor learning in the beam-walking test by comparing the slip numbers of the first and second trials (Fig. 1C). Although WT mice improved significantly in trial 2 over trial 1 (Mean ± SEM: trial 1: 0.59 ± 0.25; trial 2: 0.11 ± 0.55, $p = 0.029$), there was no significant difference between trials 1 and 2 in KO mice (Mean ± SEM: trial 1: 0.61 ± 0.16; trial 2: 0.42 ± 0.12, $p = 0.285$). Moreover, there was no significant difference in trial 1 between KO and WT littermates ($p = 0.936$). However, in trial 2, the KO mice showed more slips compared to WT mice ($p = 0.017$). These results suggest impaired motor learning in the *C9orf72* KO mice. When we analyzed motor learning further in each sex, a similar pattern was found in male *C9orf72* KO mice (Fig. 1D, Mean ± SEM: trial 1: WT: 0.42 ± 0.22; KO: 0.90 ± 0.37, trial 2: WT: 0.092 ± 0.060; KO: 0.88 ± 0.30, WT trial 1 and WT trial 2: $p = 0.072$; KO trial 1 and KO trial 2: $p = 0.95$), but not in the female mice (data not shown). Taken together, the *C9orf72* KO mice displayed motor coordination and balance deficits as well as impaired motor learning.

The gait analysis is widely used to detect cerebellar dysfunction (Ilg et al., 2007). The gait performance of *C9orf72* KO mice was further analyzed by the paw-print test. The distances of the stride, fore- and hindlimb bases, and overlap were compared between *C9orf72* KO and WT mice and were further analyzed in each sex (Fig. 1E and F). Remarkably, male KO mice displayed wider stride length compared with the WT male mice (Mean ± SEM: Total:

WT: 65.93 ± 1.36, n = 19; KO: 68.68 ± 1.25, n = 21, $p = 0.14$, Male: WT: 68.07 ± 1.48, n = 9; KO: 73.00 ± 1.33, n = 11, $p = 0.041$, Female: WT: 66.54 ± 1.95, n = 10; KO: 67.74 ± 1.96, n = 10, $p = 0.67$, mixed model). On the other hand, female KO mice and both male and female KO mice combined showed significantly decreased front base compared to WT littermates (Mean ± SEM: Total: WT: 14.71 ± 0.35, n = 19; KO: 13.29 ± 0.32, n = 21, $p = 0.0078$, Male: WT: 14.51 ± 0.54, n = 9; KO: 13.16 ± 0.47, n = 11, $p = 0.11$, Female: WT: 14.91 ± 0.46, n = 10; KO: 13.41 ± 0.46, n = 10, $p = 0.041$, mixed model). KO mice did not show any significant alterations in the hind limb base and overlap length (data not shown). These results suggest that the lack of C9orf72 protein is sufficient to produce abnormal gait.

The spontaneous locomotion of *C9orf72* KO mice was evaluated by the open-field test (Fig. 2A). Significant hyperactivity was found only in male KO mice (Mean ± SEM: Total: WT: 4171.33 ± 327.82, n = 19; KO: 4355.13 ± 309.60, n = 21, $p = 0.71$, Male: WT: 4195.82 ± 325.67, n = 9; KO: 3096.44 ± 366.03, n = 11, $p = 0.05$, Female: WT: 4670.27 ± 451.16, n = 10; KO: 4998.83 ± 451.16, n = 10, $p = 0.61$, mixed model). To determine if there is any muscular weakness, we assessed the grip strength. Interestingly, there was a significant interaction between genotype and body weight ($p = 0.032$, GENMOD with a gamma distribution) in the grip strength of the forelimbs. The grip strength data were stratified by genotype and analyzed further. The coefficient estimates of body weight showed opposite directions in the KO and WT littermates (Fig. 2B). In WT mice, heavier mice had more muscular forelimb strength as predicted. However, the relationship between body weight and forelimb strength did not exist in *C9orf72* KO mice. We then analyzed the second cohort of slightly older mice. The *C9orf72* KO male mice showed significantly decreased grip strength in forelimb than WT male littermates (Fig. 2C, Mean ± SEM: WT: 97.18 ± 4.80, n = 11; KO: 60.92 ± 12.26, n = 4, $p = 0.024$, GENMOD with a negative binomial distribution). Overall, the result suggests that *C9orf72* KO mice have hyperactivity and grip strength deficits in the forelimbs.

3.2. Hyperactivity of Purkinje cells in *C9orf72* KO mice

A growing body of literature indicates the importance of the cerebellum in ALS pathogenesis (Kaliszewska et al., 2021). Purkinje cells are the main computational neurons of the cerebellar cortex. To determine whether there is a functional alteration of Purkinje cells due to loss of C9orf72 protein, we used cell-attached patch-clamp recordings in acute brain slices to study the spontaneous firing pattern of the Purkinje cells. The mouse cerebellar Purkinje cells are known to fire spontaneously without any afferent inputs (Fig. 3A). We found a significantly higher firing frequency (Fig. 3B, Mean ± SEM: WT: 46.37 ± 3.57, n = 15; KO: 66.15 ± 6.14, n = 17, $p = 0.007$, GENMOD with a gamma distribution) and unaltered coefficient of variation (CV, a measurement of firing regularity) (Fig. 3C, Mean ± SEM: WT: 0.25 ± 0.05, n = 15; KO: 0.16 ± 0.019, n = 17, $p = 0.12$, GENMOD with a gamma distribution) in knockout Purkinje cells compared with WT littermates. These results together indicate that loss of C9orf72 led to intrinsic hyperactivity of Purkinje neurons.

3.3. Enhanced BK channel in the cerebellum of *C9orf72* KO mice

To understand the underlying causes for the increased spontaneous firing frequency of Purkinje cells in *C9orf72* KO mice, we analyzed ion channel protein levels in the cerebellum using western blot. Calcium-activated potassium channels, especially large-conductance calcium-activated potassium (BK) channels, and small-conductance calcium-activated potassium (SK) channels are known to modulate Purkinje cell firing (Swensen & Bean, 2003; Womack et al., 2009). We found that although the expression levels of SK were not statistically different between KO and WT mice (Fig. 4B, Mean ± SEM: WT: 0.28 ± 0.13, n = 6; KO: 0.24 ± 0.07, n = 7, $p = 0.47$, unpaired two-tailed t-test), the BK channel showed a significant increase (242%) in KO compared to WT mice (Fig. 4A, Mean ± SEM: WT: 0.15 ± 0.05, n = 6; KO: 0.50 ± 0.21, n = 7, $p = 0.004$, unpaired two-tailed t-test). To rule out the role of other ion channels shaping intrinsic excitability of the cerebellar Purkinje cell, we examined the resurgent sodium channels ($Na_V1.6$) and A-type K_V channels ($K_V4.3$). Both expression level were not significantly different between KO and WT mice (Suppl. Fig. 2, $Na_V1.6$: Mean ± SEM: WT: 15.43 ± 1.92, n = 5; KO: 13.94 ± 1.74, n = 9, $p = 0.59$, $K_V4.3$: WT: 4.21 ± 0.63, n = 5; KO: 6.83 ± 2.16, n = 9, $p = 0.24$, GENMOD with a gamma distribution). In summary, the western blot data suggest that increased BK channels in the *C9orf72* KO cerebellum may contribute to the increased excitability of Purkinje cells. To test this hypothesis further, we examined the effects of 1 μM NS11021, a BK channel activator, on the spontaneous firing of WT Purkinje neurons (n = 6 from 4 adult mice). There was a significant increase in frequency after drug application (Fig. 4C, Mean ± SEM: WT: 57.47 ± 5.75; KO: 75.76 ± 7.02, $p = 0.034$, GENMOD with a gamma distribution). These results together suggest that C9orf72 may play a crucial role in maintaining normal levels of BK channel activity, thereby regulating the firing properties of Purkinje cells.

3.4. Chemogenetic activation of Purkinje cells lead to motor deficits in WT mice

To investigate whether increased spike firing of Purkinje cell contributes to the motor deficits we observed in *C9orf72* KO mice, we bred *Pcp2-cre* mice with floxed DREADD (hM3Dq) mice to generate *Pcp2-cre*/hM3Dq mice to chemogenetically activate the Purkinje cell activity by CNO application (Fig. 5A). Genotyping was performed by multiplex PCR with tail DNA (Fig. 5B). hM3Dq expression was identified by a yellow mCitrine fluorescent protein expressed downstream (Zhu et al., 2016). Fluorescent images showed that hM3Dq were selectively expressed in the Purkinje cells in *Pcp2-cre*/hM3Dq mice (Fig. 5C). We further confirmed that activation of hM3Dq by bath applications of CNO (1 μM, 1 min) in brain slices led to the hyperactivity of Purkinje cells (Fig. 5D).

We then injected CNO (0.2 mg/kg) into *Pcp2-cre*/hM3Dq mice one hour before the behavioral tests. When suspended by their tails, *Pcp2-cre*/hM3Dq mice normally splayed their hind paws. There were no overt hind paw extensions or truncal arching compared to the saline group. All mice exhibited strong righting reflexes when tipped on their side. The *Pcp2-cre*/hM3Dq mice with CNO injection showed a significantly shorter latency to fall when compared with the saline-injected group (Fig. 6A, Mean ± SEM: Saline: 188.41 ± 11.03, n = 7; CNO: 76.40 ± 8.58, n = 8, $p = 0.044$, GENMOD with a gamma distribution). The beam-walking test further analyzed motor coordination and balance. The *Pcp2-cre*/hM3Dq CNO-injected group displayed a significant slip increase over the saline-injected

group (Fig. 6B, Mean ± SEM: Saline: 0.21 ± 0.12, n = 6; CNO: 1.16 ± 0.44, n = 8, p = 0.003, GENMOD with a negative binomial distribution), suggesting motor deficits induced by increased Purkinje cell firing activity. These results suggest that hyperactivity of Purkinje cells is sufficient to cause motor coordination and balance deficits found in the *C9orf72* KO mice.

4. Discussion

This study characterized an existing *C9orf72* complete KO mouse model to investigate the loss-of-function effect of C9ORF72 protein, which is also one of the three proposed disease mechanisms in ALS/FTD. We demonstrate that loss of C9orf72 led to deficits in motor coordination and balance, motor learning, gait, locomotor activity, and grip strength. In addition, we found that lack of C9orf72 protein led to increased BK channel protein level and hyperactivity of Purkinje cells in the cerebellum, a brain region poorly studied in ALS/FTD. Furthermore, applying a BK channel activator can induce similar hyperactivity of Purkinje cells found in *C9orf72* KO mice. When we used a chemogenetic method to excite the cerebellar Purkinje cell activity, WT mice recapitulated the motor coordination and balance deficits shown in *C9orf72* KO mice. Overall, these results suggest that loss of function of C9orf72 leads to abnormal motor performance and functional changes in Purkinje cells, highlighting a critical role of the cerebellum and the potential contribution of C9orf72 loss of function to the pathogenesis of ALS/FTD.

The function of the C9ORF72 protein is unknown. Loss of function of C9orf72 protein is one of the three prevalent and non-exclusive mechanisms underlying the disease. Multiple *in vivo C9orf72* knockdown (KD) and knockout (KO) animal models have been characterized (Balendra & Isaacs, 2018; Braems et al., 2020). Motor deficits are found in most *C. elegans* and zebrafish models (Butti et al., 2021; Sellier et al., 2016; Therrien et al., 2013; Yeh et al., 2018). Surprisingly, most mouse models reported normal motor function with an impaired immune system. Here, we found extensive motor impairment in accelerated rotarod, beam-walking test, gait analysis, open-field, and grip strength in a previously characterized *C9orf72* KO mouse line. Reduced latency to fall in the rotarod is consistent with the rotarod deficits found in *C9orf72* exons 2-6 knockout mice at 12 months of age (Jiang et al., 2016). Rotarod measures gross motor performance and coordination, while beam-walking can detect fine motor performance in coordination and balance. Our data suggested that in addition to abnormal coordination and balance, *C9orf72* KO mice also have impaired motor learning. We also found abnormal gait, such as increased stride and decreased front base in *C9orf72* KO mice. Significantly longer stride length also exists in SOD1 G93A mice, a widely studied ALS mouse model (Amende et al., 2005; Wooley et al., 2005). Moreover, ALS patients also have longer stride lengths but have comparable speeds to healthy subjects (Hausdorff et al., 2000). The gait problem is widely associated with cerebellar dysfunction (Ilg et al., 2007). The abnormal gaits in *C9orf72* KO mice point to a potential cerebellar dysfunction in the pathogenesis. Open-field tests measure locomotion activity. In the current study, we found loss of C9orf72 function led to hyperactivity. Such phenotype has not been reported in other KO mouse lines yet (Table 1). Interestingly, a similar phenotype has been found in a C9orf72 gain of function mouse line (Hao et al., 2019), suggesting both the loss of function and toxic gain of function of *C9orf72* mutation may disrupt the same

pathway/brain region of the motor system. Reduced grip strength is only present in a line of *C9orf72* bacterial artificial chromosome (BAC) transgenic mice (Liu et al., 2016) but was not reproduced by other groups (Mordes et al., 2020). Here, we were able to show grip strength deficits, indicating dysfunctional lower motor neurons in *C9orf72* KO mice. Finally, we observed motor deficits mostly in males. These gender-specific differences are consistent with the report that male subjects are more likely to develop ALS at a younger age (Trojsi et al., 2020; Williams et al., 2013).

Normal body weight with an enlarged spleen has been reported in most KO mouse lines. Here, in addition to an enlarged spleen, we found an age-related body weight loss in the *C9orf72* KO mice, consistent with several other loss of function models (Atanasio et al., 2016; Burberry et al., 2016; Jiang et al., 2016; Koppers et al., 2015; Sudria-Lopez et al., 2016). Weight loss has been observed in ALS patients. A recent study indicates that hypermetabolism may be an important weight loss mechanism (Wei et al., 2021). Indeed, about half of ALS patients have hypermetabolism with increased energy waste (Ahmed et al., 2016; Bouteloup et al., 2009; Steyn et al., 2018).

The cerebellum is an understudied brain region in ALS/FTD compared to upper and lower motor neurons. On the other hand, more and more studies suggest that the cerebellum is important in C9ORF72 ALS/FTD. A recently published meta-analysis presents a systematic literature search that included 72 articles on C9orf72, synapses, and the cerebellum (Kaliszewska et al., 2021). This revealed dendritic defects ($p = 0.03$) and reduced C9ORF72 in human patients ($p = 0.005$). Our current study is the first attempt to understand how the loss of function of C9orf72 leads to functional changes in the Purkinje cells and the cerebellum. We found an increased firing rate of the cerebellar Purkinje cells in the *C9orf72* KO mice. Similar electrophysiology results were reported recently in cortical neurons from patient-derived iPSCs harboring *C9ORF72* mutations (Perkins et al., 2021). Moreover, ALS patients-derived motor neurons also show hyperactivity *in vitro* (Wainger et al., 2014). These data further highlight that hyperactivity may be underlying the pathophysiology of C9ORF72 ALS/FTD.

The increased firing frequency of knockout Purkinje cells found in the cell-attached recording may be due to an alteration of Ca^{2+}-dependent K^+ currents (Swensen & Bean, 2003; Womack et al., 2009). Indeed, our western blot data uncovered increased BK channel protein in the cerebellum of a *C9orf72* KO mouse model. Furthermore, we confirmed that acute BK activator treatment could increase the firing frequency of the adult WT Purkinje cells, supporting the idea that loss of C9orf72 function leads to BK channel enhancement and further causes hyperactivity of Purkinje cells. BK channel blockers applied to rat cerebellar brain slices 13 to 21 days old (Edgerton & Reinhart, 2003) or mouse slices 20 to 35 days old (Grasselli et al., 2016) increase the Purkinje cell firing. In contrast, the BK channel KO mouse model displays a reduced firing frequency of Purkinje cells at 28 to 35 days of age (Sausbier et al., 2004). We used mice from 80 to 86 days and a BK channel activator in the manuscript. Our results are consistent with the KO mouse study but are opposite to the BK channel blocker experiments. The differences in animal age, animal species, and specific pharmacologic agents or genetic manipulations might contribute to the discrepancy between the experiments. Interestingly, BK channel transcript (KCNMA1) was

found to be significantly increased in the cerebellum of sporadic ALS patients (sALS: n = 10, 153 ± 14 reads per million, mean ± SE) compared to healthy controls (HC: n = 8, 103 ± 18, $p = 0.04$, Student's t-test), while SK channel transcript (KCNN2) is not altered (sALS: n = 10, 19 ± 2; HC: n = 8, 18 ± 1, $p = 0.47$, Student's t-test) (Prudencio et al., 2015). In a separate analysis, BK channel expression in the cerebellum of sALS patients was found to be significantly altered ($p = 0.026$) with different methylation and polyA site usage (Ebbert et al., 2017). Finally, in addition to regulating the firing, BK channels are also involved in neurodegeneration due to their localization in the inner mitochondrial membrane and regulation of mitochondrial reactive oxygen species in oxidative stress conditions (Trombetta-Lima et al., 2020). C9orf72 has been shown to be a mitochondrial inner-membrane-associated protein regulating cellular energy homeostasis via its control of oxidative phosphorylation (Wang et al., 2021). Whether BK channel expression is involved in regulating upper and lower motor neurons remains to be investigated.

We were able to recapitulate motor coordination and balance deficits found in *C9orf72* KO mice using DREADD techniques to activate Purkinje cell activity in wild-type mice, consistent with another recent report (Chao et al., 2021). We conclude that lack of C9orf72 could lead to enhanced BK channel activity, resulting in hyperactivity of the cerebellar Purkinje cells responsible for the motor deficits. Consistent with this idea, a BK channel KO mouse model displays reduced firing frequency of Purkinje cells, decreased stride length in gait analysis, and decreased movement in the open field (Sausbier et al., 2004). The results in BK KO mice match with increased Purkinje cell firing, increased stride length, and increased open field activity in the *C9orf72* KO mice. How increased Purkinje cell firing can lead to motor deficits is not known. Altered Purkinje cell firing might alter EPSP-spike coupling, as shown for SK2 channel-dependent intrinsic plasticity (Ohtsuki & Hansel, 2018). Anatomical evidence (Hoshi et al., 2005; Ichinohe et al., 2000) has demonstrated a disynaptic pathway linking the cerebellum to the striatum, which plays an essential role in motor control. Increased Purkinje cell firing likely leads to changes in striatal outputs to the motor cortex, affecting motor performance. Decreased Purkinje cell activity, abnormal social interaction, repetitive behavior, and vocalizations have been demonstrated in a mouse model of autism spectrum disorders (Tsai et al., 2012). We found similar Purkinje cell firing changes in the mouse models of DYT1 dystonia and restless legs syndrome (Liu et al., 2020; Lyu et al., 2020), highlighting that Purkinje cell and cerebellar function play a central role in neuropsychiatric diseases. Future preclinical and clinical studies using pharmacological and genetic approaches to manipulate Purkinje cell activity or target BK channel activity increase may promise to treat C9ORF72 ALS/FTD patients.

A proper mouse model is instrumental in probing the function of C9orf72, studying the ALS pathophysiology, and exploring the therapeutics of the disease. Most efforts have focused on the gain of function mouse models to study pathogenesis and therapeutics. However, a recent study on human-induced embryonic stem cell-derived motor neurons suggests that both gain- and loss-of-function mechanisms led to the neurodegeneration in C9ORF72 ALS/FTD (Shi et al., 2018). Our study indicates that loss of function alone could induce electrophysiological and motor behavioral phenotypes, suggesting a distinct role from the gain of function mechanism. Therefore, both gain- and loss-of-function of C9orf72 need to be considered when using mouse models to study the disease. It may explain why the

C9orf72 BAC mouse, a gain-of-function mouse model containing elevated C9orf72 proteins from the endogenous mouse gene, failed to develop motor behavior deficits (Mordes et al., 2020). An ideal mouse model should have both toxic repeat expansion and loss of the endogenous gene. Such mouse models have been developed and revealed that loss of function of C9orf72 in mice exacerbates motor deficits in two independent GGGGCC repeat expansion transgenic mouse models (Shao et al., 2019; Zhu et al., 2020). This strategy also has implications for C9ORF72 ALS/FTD therapeutic development by reducing the toxicities from repeat expansion while maintaining the normal allele's expression.

Supplementary Material

Refer to Web version on PubMed Central for supplementary material.

Acknowledgments

We thank the University of Florida Animal Care Services staff for animal care, Jennifer C Kirsch, Gracie Korkmaz, Maisha Anika, and Caroline Comeau for their technical assistance.

Funding

This study was supported by the National Institutes of Health grants NS82244, NS118397, and NS111498.

Abbreviations:

ACSF	artificial cerebrospinal fluid
ALS	amyotrophic lateral sclerosis
BAC	bacterial artificial chromosome
BK	large-conductance calcium-activated potassium channels
CNO	clozapine-N-oxide
CV	coefficients of variation
DPRs	dipeptide repeat proteins
DREADD	designer receptor exclusively activated by designer drugs
FTD	frontotemporal dementia
GAPDH	glyceraldehyde-3-phosphate dehydrogenase
HC	healthy control
KD	knockdown
KO	knockout
IR-DIC	infrared-differential interference contrast microscopy
PCs	Purkinje cells

RAN	repeat-associated non-ATG
sALS	sporadic ALS
SDS-PAGE	sodium dodecyl sulfate-polyacrylamide gel electrophoresis
SK	small-conductance calcium-activated potassium channels
TDP-43	TAR DNA-binding protein 43
WT	wildtype

References

Ahmed R, Irish M, Piguet O, Halliday G, Ittner L, Farooqi S, … Kiernan M (2016). Amyotrophic lateral sclerosis and frontotemporal dementia: distinct and overlapping changes in eating behaviour and metabolism. The Lancet. Neurology, 15(3). 10.1016/S1474-4422(15)00380-4

Amende I, Kale A, McCue S, Glazier S, Morgan J, & Hampton T (2005). Gait dynamics in mouse models of Parkinson's disease and Huntington's disease. Journal of neuroengineering and rehabilitation, 2. 10.1186/1743-0003-2-20

Arai T, Hasegawa M, Akiyama H, Ikeda K, Nonaka T, Mori H, … Oda T (2006). TDP-43 is a component of ubiquitin-positive tau-negative inclusions in frontotemporal lobar degeneration and amyotrophic lateral sclerosis. Biochem Biophys Res Commun, 351(3), 602–611. 10.1016/j.bbrc.2006.10.093 [PubMed: 17084815]

Ash PE, Bieniek KF, Gendron TF, Caulfield T, Lin WL, Dejesus-Hernandez M, … Petrucelli L (2013). Unconventional translation of C9ORF72 GGGGCC expansion generates insoluble polypeptides specific to c9FTD/ALS. Neuron, 77(4), 639–646. 10.1016/j.neuron.2013.02.004 [PubMed: 23415312]

Atanasio A, Decman V, White D, Ramos M, Ikiz B, Lee HC, … Lai KM (2016). C9orf72 ablation causes immune dysregulation characterized by leukocyte expansion, autoantibody production, and glomerulonephropathy in mice. Sci Rep, 6, 23204. 10.1038/srep23204 [PubMed: 26979938]

Baborie A, Griffiths TD, Jaros E, Perry R, McKeith IG, Burn DJ, … Mann DM (2015). Accumulation of dipeptide repeat proteins predates that of TDP-43 in frontotemporal lobar degeneration associated with hexanucleotide repeat expansions in C9ORF72 gene. Neuropathol Appl Neurobiol, 41(5), 601–612. 10.1111/nan.12178 [PubMed: 25185840]

Balendra R, & Isaacs AM (2018). C9orf72-mediated ALS and FTD: multiple pathways to disease. Nat Rev Neurol, 14(9), 544–558. 10.1038/s41582-018-0047-2 [PubMed: 30120348]

Belzil VV, Bauer PO, Prudencio M, Gendron TF, Stetler CT, Yan IK, … Petrucelli L (2013). Reduced C9orf72 gene expression in c9FTD/ALS is caused by histone trimethylation, an epigenetic event detectable in blood. Acta Neuropathol, 126(6), 895–905. 10.1007/s00401-013-1199-1 [PubMed: 24166615]

Bocchetta M, Cardoso MJ, Cash DM, Ourselin S, Warren JD, & Rohrer JD (2016). Patterns of regional cerebellar atrophy in genetic frontotemporal dementia. Neuroimage Clin, 11, 287–290. 10.1016/j.nicl.2016.02.008 [PubMed: 26977398]

Bouteloup C, Desport J, Clavelou P, Guy N, Derumeaux-Burel H, Ferrier A, & Couratier P (2009). Hypermetabolism in ALS patients: an early and persistent phenomenon. Journal of neurology, 256(8). 10.1007/s00415-009-5100-z

Braems E, Swinnen B, & Van Den Bosch L (2020). C9orf72 loss-of-function: a trivial, stand-alone or additive mechanism in C9 ALS/FTD? Acta neuropathologica, 140(5). 10.1007/s00401-020-02214-x

Burberry A, Suzuki N, Wang J, Moccia R, Mordes D, Stewart M, … Eggan K (2016). Loss-of-function mutations in the C9ORF72 mouse ortholog cause fatal autoimmune disease. Science translational medicine, 8(347). 10.1126/scitranslmed.aaf6038

Butti Z, Pan Y, Giacomotto J, & Patten S (2021). Reduced C9orf72 function leads to defective synaptic vesicle release and neuromuscular dysfunction in zebrafish. Communications biology, 4(1). 10.1038/s42003-021-02302-y

Carter RJ, Lione LA, Humby T, Mangiarini L, Mahal A, Bates GP, … Morton AJ (1999). Characterization of progressive motor deficits in mice transgenic for the human Huntington's disease mutation. J Neurosci, 19(8), 3248–3257. [PubMed: 10191337]

Carter RJ, Morton J, & Dunnett SB (2001). Motor coordination and balance in rodents. Curr Protoc Neurosci, *Chapter* 8, Unit 8.12. 10.1002/0471142301.ns0812s15

Cash DM, Bocchetta M, Thomas DL, Dick KM, van Swieten JC, Borroni B, … Rohrer JD (2018). Patterns of gray matter atrophy in genetic frontotemporal dementia: results from the GENFI study. Neurobiol Aging, 62, 191–196. 10.1016/j.neurobiolaging.2017.10.008 [PubMed: 29172163]

Castelnovo V, Caminiti SP, Riva N, Magnani G, Silani V, & Perani D (2019). Heterogeneous brain FDG-PET metabolic patterns in patients with C9orf72 mutation. Neurol Sci, 40(3), 515–521. 10.1007/s10072-018-3685-7 [PubMed: 30554355]

Caston J, Jones N, & Stelz T (1995). Role of preoperative and postoperative sensorimotor training on restoration of the equilibrium behavior in adult mice following cerebellectomy. Neurobiol Learn Mem, 64(3), 195–202. 10.1006/nlme.1995.0002 [PubMed: 8564373]

Chao O, Zhang H, Pathak S, Huston J, & Yang Y (2021). Functional Convergence of Motor and Social Processes in Lobule IV/V of the Mouse Cerebellum. Cerebellum (London, England). 10.1007/s12311-021-01246-7

Cistaro A, Pagani M, Montuschi A, Calvo A, Moglia C, Canosa A, … Chio A (2014). The metabolic signature of C9ORF72-related ALS: FDG PET comparison with nonmutated patients. Eur J Nucl Med Mol Imaging, 41(5), 844–852. 10.1007/s00259-013-2667-5 [PubMed: 24445987]

Cooper-Knock J, Higginbottom A, Stopford MJ, Highley JR, Ince PG, Wharton SB, … Shaw PJ (2015). Antisense RNA foci in the motor neurons of C9ORF72-ALS patients are associated with TDP-43 proteinopathy. Acta Neuropathol, 130(1), 63–75. 10.1007/s00401-015-1429-9 [PubMed: 25943887]

Corcia P, Vourc'h P, Guennoc AM, Del Mar Amador M, Blasco H, Andres C, … Meininger V (2016). Pure cerebellar ataxia linked to large C9orf72 repeat expansion. Amyotroph Lateral Scler Frontotemporal Degener, 17(3-4), 301–303. 10.3109/21678421.2015.1113298 [PubMed: 26609732]

Dang MT, Yokoi F, McNaught KS, Jengelley TA, Jackson T, Li J, & Li Y (2005). Generation and characterization of Dyt1 DeltaGAG knock-in mouse as a model for early-onset dystonia. Exp Neurol, 196(2), 452–463. 10.1016/j.expneurol.2005.08.025 [PubMed: 16242683]

DeJesus-Hernandez M, Finch NA, Wang X, Gendron TF, Bieniek KF, Heckman MG, … Rademakers R (2017). In-depth clinico-pathological examination of RNA foci in a large cohort of C9ORF72 expansion carriers. Acta Neuropathol, 134(2), 255–269. 10.1007/s00401-017-1725-7 [PubMed: 28508101]

DeJesus-Hernandez M, Mackenzie IR, Boeve BF, Boxer AL, Baker M, Rutherford NJ, … Rademakers R (2011). Expanded GGGGCC hexanucleotide repeat in noncoding region of C9ORF72 causes chromosome 9p-linked FTD and ALS. Neuron, 72(2), 245–256. 10.1016/j.neuron.2011.09.011 [PubMed: 21944778]

Donnelly CJ, Zhang PW, Pham JT, Haeusler AR, Mistry NA, Vidensky S, … Rothstein JD (2013). RNA toxicity from the ALS/FTD C9ORF72 expansion is mitigated by antisense intervention. Neuron, 80(2), 415–428. 10.1016/j.neuron.2013.10.015 [PubMed: 24139042]

Ebbert MTW, Ross CA, Pregent LJ, Lank RJ, Zhang C, Katzman RB, … Belzil VV (2017). Conserved DNA methylation combined with differential frontal cortex and cerebellar expression distinguishes C9orf72-associated and sporadic ALS, and implicates SERPINA1 in disease. Acta Neuropathol, 134(5), 715–728. 10.1007/s00401-017-1760-4 [PubMed: 28808785]

Edgerton JR, & Reinhart PH (2003). Distinct contributions of small and large conductance Ca2+-activated K+ channels to rat Purkinje neuron function. J Physiol, 548(Pt 1), 53–69. 10.1113/jphysiol.2002.027854 [PubMed: 12576503]

Fernagut PO, Diguet E, Stefanova N, Biran M, Wenning GK, Canioni P, … Tison F (2002). Subacute systemic 3-nitropropionic acid intoxication induces a distinct motor disorder in adult

C57Bl/6 mice: behavioural and histopathological characterisation. Neuroscience, 114(4), 1005–1017. [PubMed: 12379255]

Fomin V, Richard P, Hoque M, Li C, Gu Z, Fissore-O'Leary M, … Manley J (2018). The C9ORF72 Gene, Implicated in Amyotrophic Lateral Sclerosis and Frontotemporal Dementia, Encodes a Protein That Functions in Control of Endothelin and Glutamate Signaling. Molecular and cellular biology, 38(22). 10.1128/MCB.00155-18

Freibaum B, & Taylor J (2017). The Role of Dipeptide Repeats in C9ORF72-Related ALS-FTD. Frontiers in molecular neuroscience, 10. 10.3389/fnmol.2017.00035

Fremont R, Tewari A, Angueyra C, & Khodakhah K (2017). A role for cerebellum in the hereditary dystonia DYT1. Elife, 6. 10.7554/eLife.22775

Frick P, Sellier C, Mackenzie IRA, Cheng CY, Tahraoui-Bories J, Martinat C, … Neumann M (2018). Novel antibodies reveal presynaptic localization of C9orf72 protein and reduced protein levels in C9orf72 mutation carriers. Acta Neuropathol Commun, 6(1), 72. 10.1186/s40478-018-0579-0 [PubMed: 30075745]

Gendron TF, Bieniek KF, Zhang YJ, Jansen-West K, Ash PE, Caulfield T, … Petrucelli L (2013). Antisense transcripts of the expanded C9ORF72 hexanucleotide repeat form nuclear RNA foci and undergo repeat-associated non-ATG translation in c9FTD/ALS. Acta Neuropathol, 126(6), 829–844. 10.1007/s00401-013-1192-8 [PubMed: 24129584]

Gendron TF, van Blitterswijk M, Bieniek KF, Daughrity LM, Jiang J, Rush BK, … Boylan KB (2015). Cerebellar c9RAN proteins associate with clinical and neuropathological characteristics of C9ORF72 repeat expansion carriers. Acta Neuropathol, 130(4), 559–573. 10.1007/s00401-015-1474-4 [PubMed: 26350237]

Gijselinck I, Van Langenhove T, van der Zee J, Sleegers K, Philtjens S, Kleinberger G, … Van Broeckhoven C (2012). A C9orf72 promoter repeat expansion in a Flanders-Belgian cohort with disorders of the frontotemporal lobar degeneration-amyotrophic lateral sclerosis spectrum: a gene identification study. Lancet Neurol, 11(1), 54–65. 10.1016/S1474-4422(11)70261-7 [PubMed: 22154785]

Grasselli G, He Q, Wan V, Adelman JP, Ohtsuki G, & Hansel C (2016). Activity-Dependent Plasticity of Spike Pauses in Cerebellar Purkinje Cells. Cell Rep, 14(11), 2546–2553. 10.1016/j.celrep.2016.02.054 [PubMed: 26972012]

Hao Z, Liu L, Tao Z, Wang R, Ren H, Sun H, … Wang G (2019). Motor dysfunction and neurodegeneration in a C9orf72 mouse line expressing poly-PR. Nat Commun, 10(1), 2906. 10.1038/s41467-019-10956-w [PubMed: 31266945]

Hardiman O, Al-Chalabi A, Chio A, Corr EM, Logroscino G, Robberecht W, … van den Berg LH (2017). Amyotrophic lateral sclerosis. Nat Rev Dis Primers, 3, 17071. 10.1038/nrdp.2017.71 [PubMed: 28980624]

Hausdorff J, Lertratanakul A, Cudkowicz M, Peterson A, Kaliton D, & Goldberger A (2000). Dynamic markers of altered gait rhythm in amyotrophic lateral sclerosis. Journal of applied physiology (Bethesda, Md. : 1985), 88(6). 10.1152/jappl.2000.88.6.2045

Hornberger M. (2012). Assessment of psychiatric changes in C9ORF72 frontotemporal dementia. Alzheimers Res Ther, 4(6), 49. 10.1186/alzrt152 [PubMed: 23269019]

Hoshi E, Tremblay L, Feger J, Carras PL, & Strick PL (2005). The cerebellum communicates with the basal ganglia. Nat Neurosci, 8(11), 1491–1493. [PubMed: 16205719]

Ichinohe N, Mori F, & Shoumura K (2000). A di-synaptic projection from the lateral cerebellar nucleus to the laterodorsal part of the striatum via the central lateral nucleus of the thalamus in the rat. Brain Res, 880(1-2), 191–197. [PubMed: 11033006]

Ilg W, Golla H, Thier P, & Giese M (2007). Specific influences of cerebellar dysfunctions on gait. Brain : a journal of neurology, 130(Pt 3). 10.1093/brain/awl376

Irwin DJ, McMillan CT, Brettschneider J, Libon DJ, Powers J, Rascovsky K, … Grossman M (2013). Cognitive decline and reduced survival in C9orf72 expansion frontotemporal degeneration and amyotrophic lateral sclerosis. J Neurol Neurosurg Psychiatry, 84(2), 163–169. 10.1136/jnnp-2012-303507 [PubMed: 23117491]

Ito M. (2008). Control of mental activities by internal models in the cerebellum. Nat Rev Neurosci, 9(4), 304–313. 10.1038/nrn2332 [PubMed: 18319727]

Jiang J, Zhu Q, Gendron TF, Saberi S, McAlonis-Downes M, Seelman A, … Lagier-Tourenne C (2016). Gain of Toxicity from ALS/FTD-Linked Repeat Expansions in C9ORF72 Is Alleviated by Antisense Oligonucleotides Targeting GGGGCC-Containing RNAs. Neuron, 90(3), 535–550. 10.1016/j.neuron.2016.04.006 [PubMed: 27112497]

Kaliszewska A, Allison J, Col T, Shaw C, & Arias N (2021). Elucidating the Role of Cerebellar Synaptic Dysfunction in C9orf72-ALS/FTD - a Systematic Review and Meta-Analysis. Cerebellum (London, England). 10.1007/s12311-021-01320-0

Koppers M, Blokhuis A, Westeneng H, Terpstra M, Zundel C, Vieira de Sá R, … Pasterkamp R (2015). C9orf72 ablation in mice does not cause motor neuron degeneration or motor deficits. Annals of neurology, 78(3). 10.1002/ana.24453

Lagier-Tourenne C, Baughn M, Rigo F, Sun S, Liu P, Li HR, … Ravits J (2013). Targeted degradation of sense and antisense C9orf72 RNA foci as therapy for ALS and frontotemporal degeneration. Proc Natl Acad Sci U S A, 110(47), E4530–4539. 10.1073/pnas.1318835110 [PubMed: 24170860]

Lakshmana M, Chung J, Wickramarachchi S, Tak E, Bianchi E, Koo E, & Kang D (2010). A fragment of the scaffolding protein RanBP9 is increased in Alzheimer's disease brains and strongly potentiates amyloid-beta peptide generation. FASEB journal : official publication of the Federation of American Societies for Experimental Biology, 24(1). 10.1096/fj.09-136457

Lalonde R, Bensoula AN, & Filali M (1995). Rotorod sensorimotor learning in cerebellar mutant mice. - PubMed - NCBI. Neurosci Res, 22(4), 423–426. 10.1016/0168-0102(95)00916-h [PubMed: 7478307]

Liu Y, Pattamatta A, Zu T, Reid T, Bardhi O, Borchelt DR, … Ranum LP (2016). C9orf72 BAC Mouse Model with Motor Deficits and Neurodegenerative Features of ALS/FTD. Neuron, 90(3), 521–534. 10.1016/j.neuron.2016.04.005 [PubMed: 27112499]

Liu Y, Xing H, Sheng W, Singh K, Korkmaz A, Comeau C, … Li Y (2021). Alteration of the cholinergic system and motor deficits in cholinergic neuron-specific Dyt1 knockout mice. Neurobiology of disease. 10.1016/j.nbd.2021.105342

Liu Y, Xing H, Wilkes B, Yokoi F, Chen H, Vaillancourt D, & Li Y (2020). The abnormal firing of Purkinje cells in the knockin mouse model of DYT1 dystonia. Brain research bulletin, 165. 10.1016/j.brainresbull.2020.09.011

Lyu S, Xing H, DeAndrade MP, Liu Y, Perez PD, Yokoi F, … Li Y (2019). The role of BTBD9 in striatum and restless legs syndrome. eNeuro, 0277–0219. 10.1523/eneuro.0277-19.2019

Lyu S, Xing H, DeAndrade MP, Perez PD, Yokoi F, Febo M, … Li Y (2020). The Role of BTBD9 in the Cerebellum, Sleep-like Behaviors and the Restless Legs Syndrome. Neuroscience, 440, 85–96. 10.1016/j.neuroscience.2020.05.021 [PubMed: 32446853]

Mackenzie IR, Frick P, Grasser FA, Gendron TF, Petrucelli L, Cashman NR, … Neumann M (2015). Quantitative analysis and clinico-pathological correlations of different dipeptide repeat protein pathologies in C9ORF72 mutation carriers. Acta Neuropathol, 130(6), 845–861. 10.1007/s00401-015-1476-2 [PubMed: 26374446]

MacLaren DA, Browne RW, Shaw JK, Krishnan Radhakrishnan S, Khare P, Espana RA, & Clark SD (2016). Clozapine N-Oxide Administration Produces Behavioral Effects in Long-Evans Rats: Implications for Designing DREADD Experiments. eNeuro, 3(5). 10.1523/eneuro.0219-16.2016

Mahoney CJ, Downey LE, Ridgway GR, Beck J, Clegg S, Blair M, … Warren JD (2012). Longitudinal neuroimaging and neuropsychological profiles of frontotemporal dementia with C9ORF72 expansions. Alzheimers Res Ther, 4(5), 41. 10.1186/alzrt144 [PubMed: 23006986]

Majounie E, Renton AE, Mok K, Dopper EG, Waite A, Rollinson S, … Traynor BJ (2012). Frequency of the C9orf72 hexanucleotide repeat expansion in patients with amyotrophic lateral sclerosis and frontotemporal dementia: a cross-sectional study. Lancet Neurol, 11(4), 323–330. 10.1016/s1474-4422(12)70043-1 [PubMed: 22406228]

Mann DM, Rollinson S, Robinson A, Bennion Callister J, Thompson JC, Snowden JS, … Pickering-Brown S (2013). Dipeptide repeat proteins are present in the p62 positive inclusions in patients with frontotemporal lobar degeneration and motor neurone disease associated with expansions in C9ORF72. Acta Neuropathol Commun, 1, 68. 10.1186/2051-5960-1-68 [PubMed: 24252525]

Meloni M, Farris R, Solla P, Mascia MM, Marrosu F, & Cannas A (2017). C9ORF72 Intermediate Repeat Expansion in a Patient With Psychiatric Disorders and Progressive Cerebellar Ataxia. Neurologist, 22(6), 245–246. 10.1097/nrl.0000000000000147 [PubMed: 29095328]

Mizielinska S, Lashley T, Norona FE, Clayton EL, Ridler CE, Fratta P, & Isaacs AM (2013). C9orf72 frontotemporal lobar degeneration is characterised by frequent neuronal sense and antisense RNA foci. Acta Neuropathol, 126(6), 845–857. 10.1007/s00401-013-1200-z [PubMed: 24170096]

Mordes D, Morrison B, Ament X, Cantrell C, Mok J, Eggan P, … Rothstein J (2020). Absence of Survival and Motor Deficits in 500 Repeat C9ORF72 BAC Mice. Neuron, 108(4). 10.1016/j.neuron.2020.08.009

Mori K, Weng SM, Arzberger T, May S, Rentzsch K, Kremmer E, … Edbauer D (2013). The C9orf72 GGGGCC repeat is translated into aggregating dipeptide-repeat proteins in FTLD/ALS. Science, 339(6125), 1335–1338. 10.1126/science.1232927 [PubMed: 23393093]

Neumann M, Sampathu D, Kwong L, Truax A, Micsenyi M, Chou T, … Lee V (2006). Ubiquitinated TDP-43 in frontotemporal lobar degeneration and amyotrophic lateral sclerosis. Science (New York, N.Y.), 314(5796). 10.1126/science.1134108

Nguon K, Ladd B, Baxter MG, & Sajdel-Sulkowska EM (2005). Sexual dimorphism in cerebellar structure, function, and response to environmental perturbations. Prog Brain Res, 148, 341–351. 10.1016/s0079-6123(04)48027-3 [PubMed: 15661202]

O'Rourke JG, Bogdanik L, Yanez A, Lall D, Wolf AJ, Muhammad AK, … Baloh RH (2016). C9orf72 is required for proper macrophage and microglial function in mice. Science, 351(6279), 1324–1329. 10.1126/science.aaf1064 [PubMed: 26989253]

Ohtsuki G, & Hansel C (2018). Synaptic Potential and Plasticity of an SK2 Channel Gate Regulate Spike Burst Activity in Cerebellar Purkinje Cells. iScience, 1, 49–54. 10.1016/j.isci.2018.02.001 [PubMed: 29888747]

Olney NT, Spina S, & Miller BL (2017). Frontotemporal Dementia. Neurol Clin, 35(2), 339–374. 10.1016/j.ncl.2017.01.008 [PubMed: 28410663]

Pang W, & Hu F (2021). Cellular and physiological functions of C9ORF72 and implications for ALS/FTD. Journal of neurochemistry, 157(3). 10.1111/jnc.15255

Panman JL, Jiskoot LC, Bouts M, Meeter LHH, van der Ende EL, Poos JM, … Papma JM (2019). Gray and white matter changes in presymptomatic genetic frontotemporal dementia: a longitudinal MRI study. Neurobiol Aging, 76, 115–124. 10.1016/j.neurobiolaging.2018.12.017 [PubMed: 30711674]

Papma JM, Jiskoot LC, Panman JL, Dopper EG, den Heijer T, Donker Kaat L, … van Swieten JC (2017). Cognition and gray and white matter characteristics of presymptomatic C9orf72 repeat expansion. Neurology, 89(12), 1256–1264. 10.1212/wnl.0000000000004393 [PubMed: 28855404]

Perkins E, Burr K, Banerjee P, Mehta A, Dando O, Selvaraj B, … Livesey M (2021). Altered network properties in C9ORF72 repeat expansion cortical neurons are due to synaptic dysfunction. Molecular neurodegeneration, 16(1). 10.1186/s13024-021-00433-8

Prell T, & Grosskreutz J (2013). The involvement of the cerebellum in amyotrophic lateral sclerosis. Amyotroph Lateral Scler Frontotemporal Degener, 14(7-8), 507–515. 10.3109/21678421.2013.812661 [PubMed: 23889583]

Prudencio M, Belzil VV, Batra R, Ross CA, Gendron TF, Pregent LJ, … Petrucelli L (2015). Distinct brain transcriptome profiles in C9orf72-associated and sporadic ALS. Nat Neurosci, 18(8), 1175–1182. 10.1038/nn.4065 [PubMed: 26192745]

Ramos-Campoy O, Avila-Polo R, Grau-Rivera O, Antonell A, Clarimon J, Rojas-Garcia R, … Gelpi E (2018). Systematic Screening of Ubiquitin/p62 Aggregates in Cerebellar Cortex Expands the Neuropathological Phenotype of the C9orf72 Expansion Mutation. J Neuropathol Exp Neurol, 77(8), 703–709. 10.1093/jnen/nly047 [PubMed: 29889265]

Renton AE, Majounie E, Waite A, Simon-Sanchez J, Rollinson S, Gibbs JR, … Traynor BJ (2011). A hexanucleotide repeat expansion in C9ORF72 is the cause of chromosome 9p21-linked ALS-FTD. Neuron, 72(2), 257–268. 10.1016/j.neuron.2011.09.010 [PubMed: 21944779]

Sausbier M, Hu H, Arntz C, Feil S, Kamm S, Adelsberger H, … Ruth P (2004). Cerebellar ataxia and Purkinje cell dysfunction caused by Ca2+-activated K+ channel deficiency. Proc Natl Acad Sci U S A, 101(25), 9474–9478. 10.1073/pnas.0401702101 [PubMed: 15194823]

Sellier C, Campanari M, Julie Corbier C, Gaucherot A, Kolb-Cheynel I, Oulad-Abdelghani M, … Charlet-Berguerand N (2016). Loss of C9ORF72 impairs autophagy and synergizes with polyQ Ataxin-2 to induce motor neuron dysfunction and cell death. The EMBO journal, 35(12). 10.15252/embj.201593350

Shao Q, Liang C, Chang Q, Zhang W, Yang M, & Chen J (2019). C9orf72 deficiency promotes motor deficits of a C9ALS/FTD mouse model in a dose-dependent manner. Acta neuropathologica communications, 7(1). 10.1186/s40478-019-0685-7

Shi Y, Lin S, Staats K, Li Y, Chang W, Hung S, … Ichida J (2018). Haploinsufficiency leads to neurodegeneration in C9ORF72 ALS/FTD human induced motor neurons. Nature medicine, 24(3). 10.1038/nm.4490

Sivadasan R, Hornburg D, Drepper C, Frank N, Jablonka S, Hansel A, … Sendtner M (2016). C9ORF72 interaction with cofilin modulates actin dynamics in motor neurons. Nature neuroscience, 19(12). 10.1038/nn.4407

Steyn F, Ioannides Z, van Eijk R, Heggie S, Thorpe K, Ceslis A, … Ngo S (2018). Hypermetabolism in ALS is associated with greater functional decline and shorter survival. Journal of neurology, neurosurgery, and psychiatry, 89(10). 10.1136/jnnp-2017-317887

Sudria-Lopez E, Koppers M, de Wit M, van der Meer C, Westeneng H, Zundel C, … Pasterkamp R (2016). Full ablation of C9orf72 in mice causes immune system-related pathology and neoplastic events but no motor neuron defects. Acta neuropathologica, 132(1). 10.1007/s00401-016-1581-x

Swensen A, & Bean B (2003). Ionic Mechanisms of Burst Firing in Dissociated Purkinje Neurons. The Journal of neuroscience : the official journal of the Society for Neuroscience, 23(29). 10.1523/JNEUROSCI.23-29-09650.2003

Swinnen B, Robberecht W, & Van Den Bosch L (2020). RNA toxicity in non-coding repeat expansion disorders. The EMBO journal, 39(1). 10.15252/embj.2018101112

Tan RH, Devenney E, Dobson-Stone C, Kwok JB, Hodges JR, Kiernan MC, … Hornberger M (2014). Cerebellar integrity in the amyotrophic lateral sclerosis-frontotemporal dementia continuum. PLoS One, 9(8), e105632. 10.1371/journal.pone.0105632 [PubMed: 25144223]

Therrien M, Rouleau G, Dion P, & Parker J (2013). Deletion of C9ORF72 results in motor neuron degeneration and stress sensitivity in C. elegans. PloS one, 8(12). 10.1371/journal.pone.0083450

Trojsi F, D'Alvano G, Bonavita S, & Tedeschi G (2020). Genetics and Sex in the Pathogenesis of Amyotrophic Lateral Sclerosis (ALS): Is There a Link? Int J Mol Sci, 21(10). 10.3390/ijms21103647

Trombetta-Lima M, Krabbendam IE, & Dolga AM (2020). Calcium-activated potassium channels: implications for aging and age-related neurodegeneration. Int J Biochem Cell Biol, 123, 105748. 10.1016/j.biocel.2020.105748 [PubMed: 32353429]

Tsai PT, Hull C, Chu Y, Greene-Colozzi E, Sadowski AR, Leech JM, … Sahin M (2012). Autistic-like behaviour and cerebellar dysfunction in Purkinje cell Tsc1 mutant mice. Nature, 488(7413), 647–651. 10.1038/nature11310 [PubMed: 22763451]

van Blitterswijk M, Gendron TF, Baker MC, DeJesus-Hernandez M, Finch NA, Brown PH, … Rademakers R (2015). Novel clinical associations with specific C9ORF72 transcripts in patients with repeat expansions in C9ORF72. Acta Neuropathol, 130(6), 863–876. 10.1007/s00401-015-1480-6 [PubMed: 26437865]

Voelkl B, Altman NS, Forsman A, Forstmeier W, Gurevitch J, Jaric I, … Würbel H (2020). Reproducibility of animal research in light of biological variation. Nat Rev Neurosci, 21(7), 384–393. 10.1038/s41583-020-0313-3 [PubMed: 32488205]

Wainger BJ, Kiskinis E, Mellin C, Wiskow O, Han SS, Sandoe J, … Woolf CJ (2014). Intrinsic membrane hyperexcitability of amyotrophic lateral sclerosis patient-derived motor neurons. Cell Rep, 7(1), 1–11. 10.1016/j.celrep.2014.03.019 [PubMed: 24703839]

Waite AJ, Baumer D, East S, Neal J, Morris HR, Ansorge O, & Blake DJ (2014). Reduced C9orf72 protein levels in frontal cortex of amyotrophic lateral sclerosis and frontotemporal degeneration brain with the C9ORF72 hexanucleotide repeat expansion. Neurobiol Aging, 35(7), 1779.e1775–1779.e1713. 10.1016/j.neurobiolaging.2014.01.016

Wang R, Wang H, Carrera I, Xu S, & Lakshmana M (2015). COPS5 protein overexpression increases amyloid plaque burden, decreases spinophilin-immunoreactive puncta, and exacerbates learning

and memory deficits in the mouse brain. The Journal of biological chemistry, 290(14). 10.1074/jbc.M114.595926

Wang T, Liu H, Itoh K, Oh S, Zhao L, Murata D, … Wang J (2021). C9orf72 regulates energy homeostasis by stabilizing mitochondrial complex I assembly. Cell Metab, 33(3), 531–546.e539. 10.1016/j.cmet.2021.01.005 [PubMed: 33545050]

Wei Q, Ou R, Cao B, Chen Y, Hou Y, Zhang L, … Shang H (2021). Early weight instability is associated with cognitive decline and poor survival in amyotrophic lateral sclerosis. Brain research bulletin, 171. 10.1016/j.brainresbull.2021.02.022

Williams KL, Fifita JA, Vucic S, Durnall JC, Kiernan MC, Blair IP, & Nicholson GA (2013). Pathophysiological insights into ALS with C9ORF72 expansions. J Neurol Neurosurg Psychiatry, 84(8), 931–935. 10.1136/jnnp-2012-304529 [PubMed: 23463871]

Womack MD, Hoang C, & Khodakhah K (2009). Large conductance calcium-activated potassium channels affect both spontaneous firing and intracellular calcium concentration in cerebellar Purkinje neurons. Neuroscience, 162(4), 989–1000. 10.1016/j.neuroscience.2009.05.016 [PubMed: 19446607]

Wooley C, Sher R, Kale A, Frankel W, Cox G, & Seburn K (2005). Gait analysis detects early changes in transgenic SOD1(G93A) mice. Muscle & nerve, 32(1). 10.1002/mus.20228

Xiao S, MacNair L, McGoldrick P, McKeever PM, McLean JR, Zhang M, … Robertson J (2015). Isoform-specific antibodies reveal distinct subcellular localizations of C9orf72 in amyotrophic lateral sclerosis. Ann Neurol, 78(4), 568–583. 10.1002/ana.24469 [PubMed: 26174152]

Yeh T, Liu H, Li Y, Lu C, Shih H, Chiu C, … Cheng Y (2018). C9orf72 is essential for neurodevelopment and motility mediated by Cyclin G1. Experimental neurology, 304. 10.1016/j.expneurol.2018.03.002

Yokoi F, Dang MT, Li J, Standaert DG, & Li Y (2011). Motor deficits and decreased striatal dopamine receptor 2 binding activity in the striatum-specific Dyt1 conditional knockout mice. PLoS One, 6(9), e24539. 10.1371/journal.pone.0024539 [PubMed: 21931745]

Yokoi F, Oleas J, Xing H, Liu Y, Dexter KM, Misztal C, … Li Y (2020). Decreased number of striatal cholinergic interneurons and motor deficits in dopamine receptor 2-expressing-cell-specific Dyt1 conditional knockout mice. Neurobiol Dis, 134, 104638. 10.1016/j.nbd.2019.104638 [PubMed: 31618684]

Yokoi F, Yang G, Li J, DeAndrade MP, Zhou T, & Li Y (2010). Earlier onset of motor deficits in mice with double mutations in Dyt1 and Sgce. J Biochem, 148(4), 459–466. 10.1093/jb/mvq078 [PubMed: 20627944]

Zhang XM, Ng AH, Tanner JA, Wu WT, Copeland NG, Jenkins NA, & Huang JD (2004). Highly restricted expression of Cre recombinase in cerebellar Purkinje cells. Genesis, 40(1), 45–51. 10.1002/gene.20062 [PubMed: 15354293]

Zhu H, Aryal DK, Olsen RH, Urban DJ, Swearingen A, Forbes S, … Hochgeschwender U (2016). Cre-dependent DREADD (Designer Receptors Exclusively Activated by Designer Drugs) mice. Genesis, 54(8), 439–446. 10.1002/dvg.22949 [PubMed: 27194399]

Zhu Q, Jiang J, Gendron T, McAlonis-Downes M, Jiang L, Taylor A, … Cleveland D (2020). Reduced C9ORF72 function exacerbates gain of toxicity from ALS/FTD-causing repeat expansion in C9orf72. Nature neuroscience, 23(5). 10.1038/s41593-020-0619-5

Zu T, Liu Y, Banez-Coronel M, Reid T, Pletnikova O, Lewis J, … Ranum LP (2013). RAN proteins and RNA foci from antisense transcripts in C9ORF72 ALS and frontotemporal dementia. Proc Natl Acad Sci U S A, 110(51), E4968–4977. 10.1073/pnas.1315438110 [PubMed: 24248382]

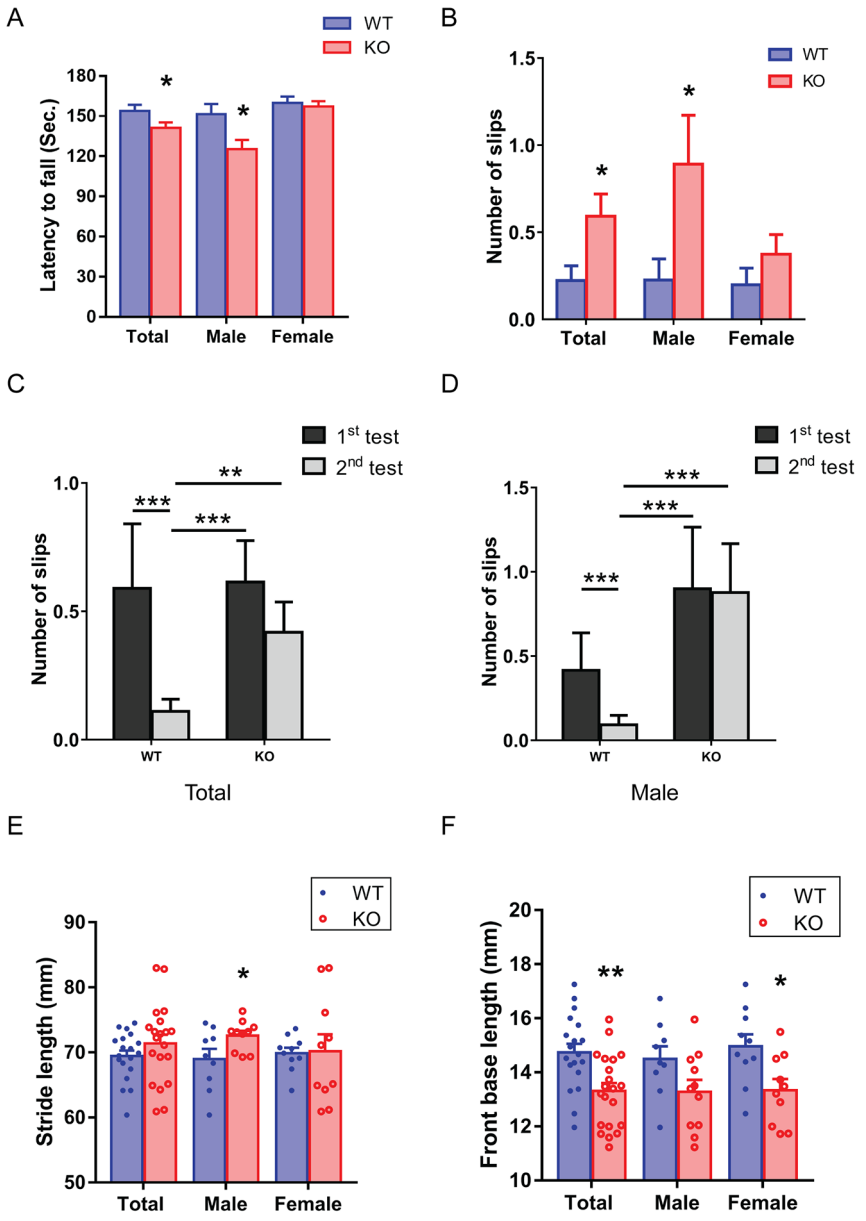

FIG 1.

Impaired coordination and balance in *C9orf72* KO mice. (A) In the accelerated rotarod test, *C9orf72* KO mice showed a significantly decreased latency to fall than WT mice in the male group and when both sexes were combined; however, there was no significant difference in the latency to fall between female WT and *C9orf72* KO mice. Male: 9 WT, 11 KO, average age: 113 days, range: 75-156 days. Female: 10 WT, 10 KO, average age: 121 days, range 84-162 days. Total: 19 WT, 21 KO, average age: 117 days, range 75-162 days. (B) In the beam-walking test, *C9orf72* KO mice showed a significant increase in slip numbers in the male group and when both sexes were combined. On the other hand, there was no significant difference in slip numbers between female WT and *C9orf72* KO mice. Male: 9 WT, 11 KO, average age: 129 days, range 91-172 days. Female: 10 WT, 10 KO, average age: 137 days, range 100-178 days. Total: 19 WT, 21 KO, average age: 133 days, range 91-178 days). (C)

In the first trial of the beam-walking test, *C9orf72* KO mice performed comparably to WT mice. While in the second trial, *C9orf72* KO mice displayed excessive slips compared to WT littermates. When comparing two trials, *C9orf72* KO mice didn't improve in the second trial, but their WT littermates showed significant improvement or motor learning. (D) Male *C9orf72* KO mice didn't have improved performance in the second trial, while the male WT mice displayed improved performance. Gait analysis showed increased stride length in the male *C9orf72* KO mice (E) and decreased front base length in the total and female groups (F). Male: 9 WT, 11 KO, average age: 149 days, range 111-192 days. Female: 10 WT, 10 KO, average age: 157 days, range 120-198 days. Total: 19 WT, 21 KO, average age: 153 days, range 111-198 days. Bars represent mean ± SEM. *$p < 0.05$, **$p < 0.01$, ***$p < 0.001$.

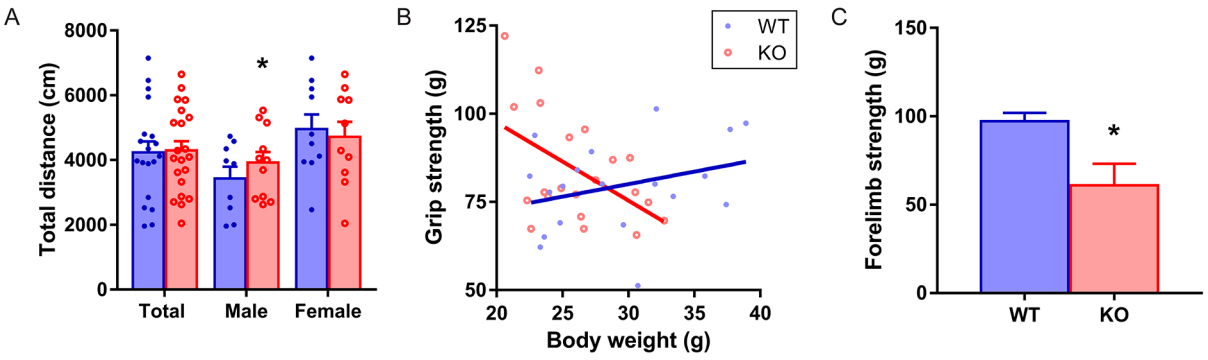

FIG 2.

Hyperactivity and abnormal grip strength of the *C9orf72* KO mice. (A) *C9orf72* KO mice displayed increased total distance in the open field test. Male: 9 WT, 11 KO, average age: 137 days, range 99-180 days. Female: 10 WT, 10 KO, average age: 145 days, range 108-186 days. Total: 19 WT, 21 KO, average age: 141 days, range 99-186 days. (B) A significant interaction between genotype and body weight in the grip strength of forelimbs. In WT mice, heavier mice have stronger forelimb strength. However, such a relationship did not exist in *C9orf72* KO mice. Bars represent mean ± SEMMale: 9 WT, 11 KO, average age: 183 days, range 145-226 days. Female: 10 WT, 10 KO, average age: 191 days, range 154-232 days. Total: 19 WT, 21 KO, average age: 187 days, range 145-232 days. (C) In a second cohort, the C9orf72 KO male mice showed a significantly decreased forelimb grip strength than WT male littermates. Male: 11 WT, 4 KO, average age: 238 days, range 198-269 days. . *$p < 0.05$.

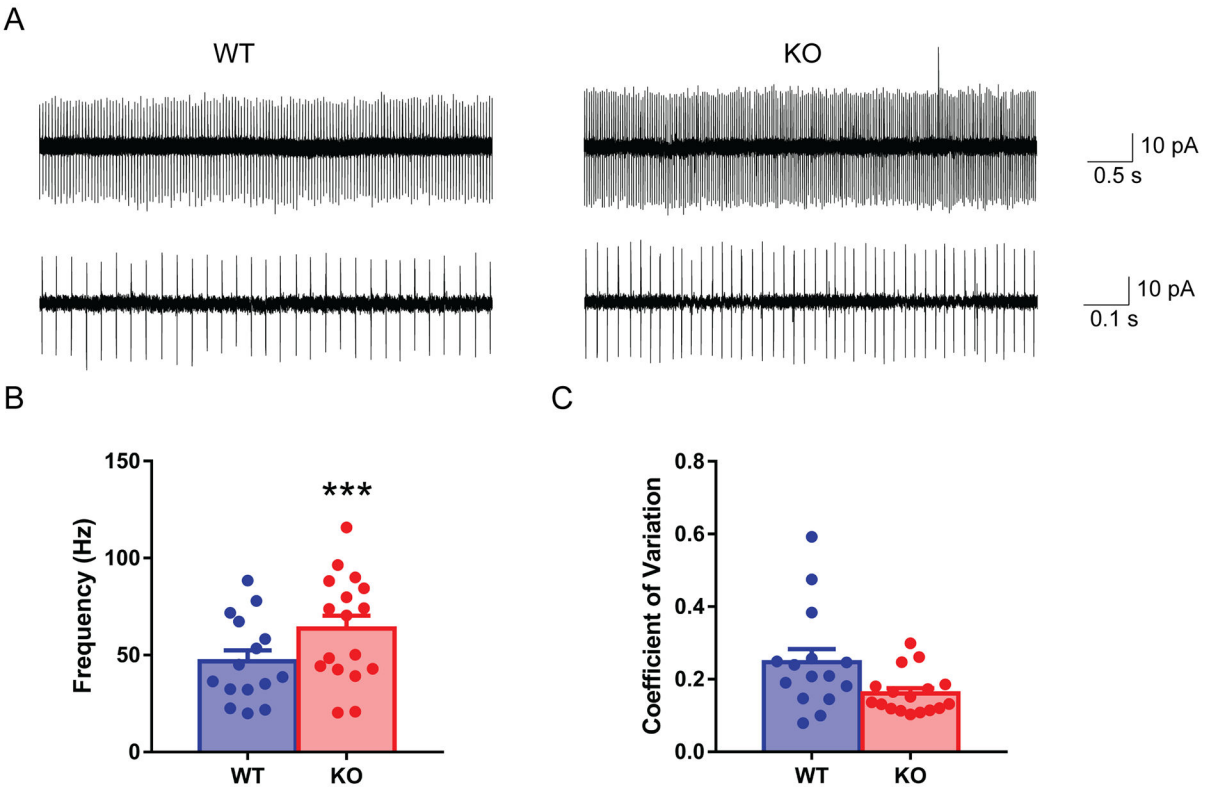

FIG 3.

Hyperactivity of Purkinje cells in *C9orf72* KO mice. Sample traces show the spontaneous firing of Purkinje cells in cell-attached mode recording (A). Purkinje cells from *C9orf72* KO mice had a higher firing rate (B) and an unchanged coefficient of variation (C). 4 WT male mice, 15 cells; 3 KO male mice, 17 cells, average age: 93 days, 87-103 days. Bars represent mean ± SEM. ***$p < 0.001$.

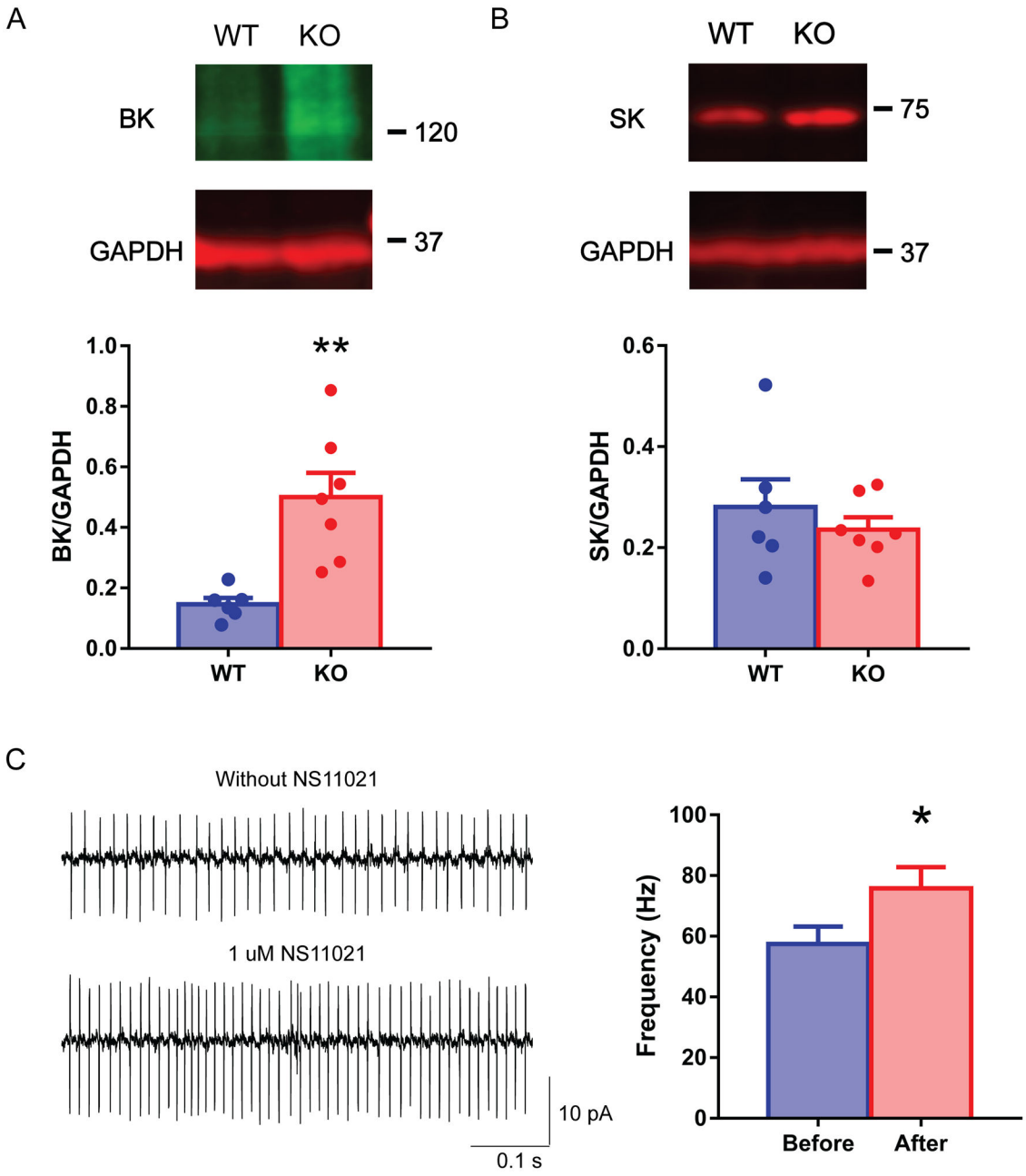

FIG 4.

Increased BK channel in *C9orf72* KO mice. Representative Western blot images (top) and their quantifications (bottom) of the cerebellar tissue samples (6 WT male mice, 7 KO male mice, average age: 256 days, range 215-296 days). *C9orf72* KO mice showed a higher level of the cerebellar BK channels (A) than WT mice. On the other hand, *C9orf72* KO mice did not significantly differ in SK channels (B). Cell-attached recording of tonic Purkinje cells before and after NS11021 application. There is a significant increase in the firing frequency (C) in the adult WT tonic Purkinje cells. The bar graphs show mean ± standard errors. *$p < 0.05$, **$p < 0.01$.

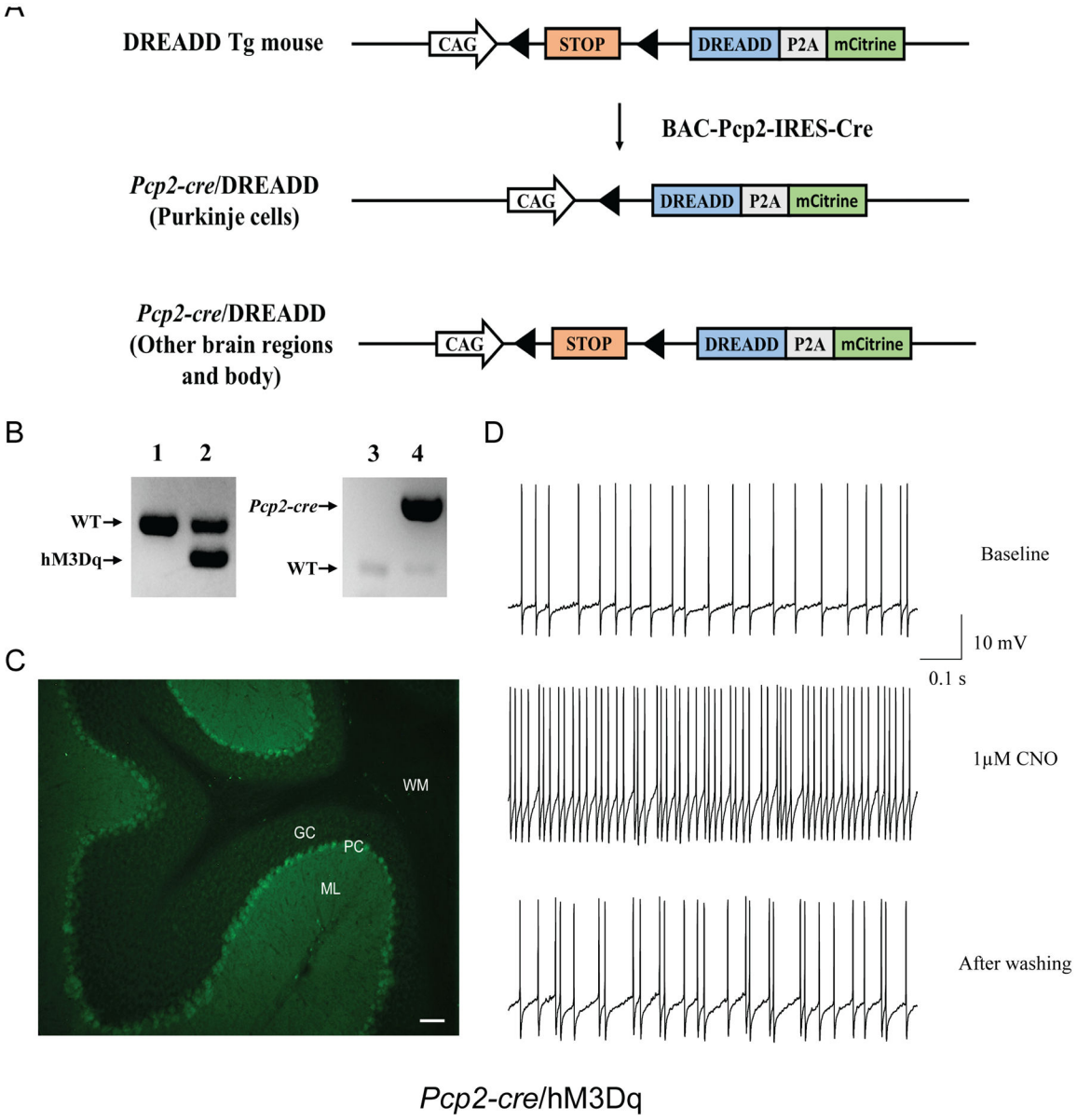

FIG 5.

Generation of *Pcp2-cre*/hM3Dq mice. (A) Strategies to generate *Pcp2-cre*/DREADD mice. Floxed DREADD mice were crossed with *Pcp2-cre* mice to produce *Pcp2-cre*/DREADD mice. (B) Representative PCR-based genotyping results for *Pcp2-cre*/hM3Dq mice. Lanes 1 and 3: WT mouse; Lane 2: hM3Dq heterozygous mouse; Lane 4: *Pcp2-cre* mouse. (C) Representative images of cerebellum sagittal slices from *Pcp2-cre*/hM3Dq mice with DREADD expression in the Purkinje cells. (D) Chemogenetic manipulation of Purkinje cell activity *in vitro*. Representative Purkinje cell recording traces from *Pcp2-cre*/hM3Dq before (top), during, and after CNO bath application (bottom). GC: granule cell; WM: white matter; PC: Purkinje cell; ML: molecular layer. Scale bar represents 100 μm.

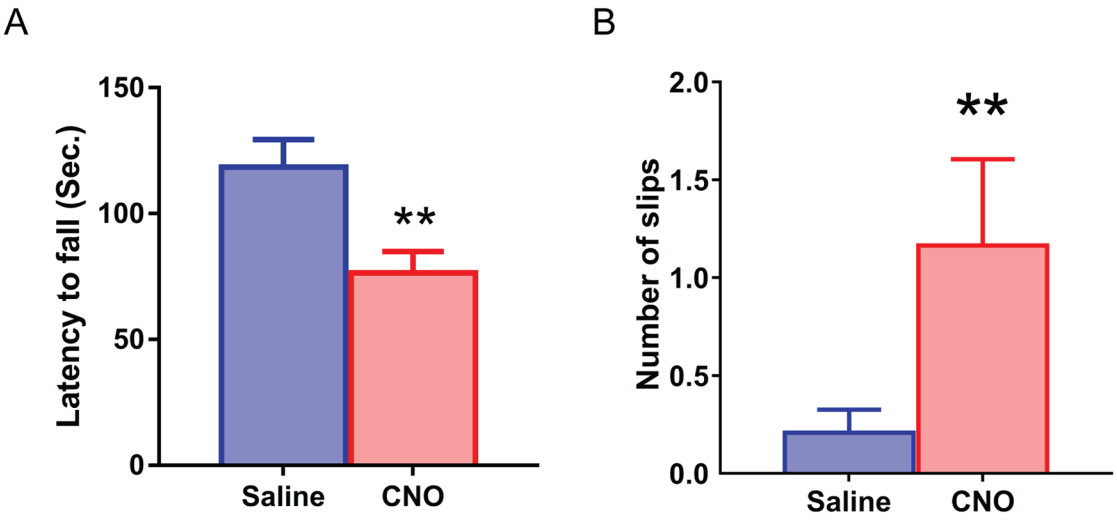

FIG 6.

Rotarod and beam-walking deficits in *Pcp2-cre*/hM3Dq mice after CNO injection. Males: 6 CNO group, 6 saline group, average age: 152 days, range 62-205 days; Female: 2 CNO group, 3 saline group, average age: 137 days, range 62-205 days). *Pcp2-cre*/hM3Dq mice, after CNO injection, showed decreased latency to fall (A) and displayed excessive slips as they crossed the beam (B) compared to the saline-injected group. 1–6: trial number. Bars represent mean ± SEM. $^{**}p < 0.01$.

Table 1.

Motor deficits comparison of C9orf72 knockout mouse models.

Reference	Body weight	Rotarod	Grip Strength	Gait analysis	Locomotion
(Koppers et al., 2015)	Subtle decrease	Normal	Normal	NA	NA
(Sudria-Lopez et al., 2016)	Subtle decrease	Normal	Normal	NA	NA
(Atanasio et al., 2016)	Decrease	Normal	NA	Abnormal	Decrease
(Jiang et al., 2016)	Subtle decrease	Reduced	Normal	Normal	Normal
(O'Rourke et al., 2016)	Normal	Normal	Normal	NA	Decrease
Our study	Subtle decrease	Decrease	Decrease	Abnormal	Increase